Horizontal Flow Boiling Of Single Component And Binary Refrigerant Mixtures

---

ER-8006-2
Research Project 2792-09

Prepared by
National Institute of Standards and Technology
Building and Fire Research Laboratory
Gaithersburg, MD 20899

Authors and Principal Investigators
M.A. Kedzierski and D.A. Didion

Prepared for
Electrical Power Research Institute
3412 Hillview Avenue
Palo Alto, California 94304

EPRI Project Manager
J. Kim

Exploratory Research Program
Nuclear Power Division
Office of Exploratory Research

ABSTRACT

This report contains three studies on refrigerant mixture heat transfer funded by N.I.S.T. and E.P.R.I. (RP 80006-2). The first study, VISUALIZATION OF NUCLEATE FLOW FOR AN R22/R114 MIXTURE AND ITS COMPONENTS, is presented in section 1. It investigates the phenomena of the suppression of nucleation due to increased mass flow while all other conditions are fixed. This study also compares the nucleate activity of the binary mixture to the nucleate activity of the pure components. The fluids investigated are a 37.7% mole R114 binary mixture and the individual components R22 and R114.

The second study, CAUSES OF THE APPARENT HEAT TRANSFER DEGRADATION FOR REFRIGERANT MIXTURES, is presented in section 2. It investigates the causes of the apparent heat transfer degradation associated with horizontal - annular flow evaporation of refrigerant mixtures. For horizontal-annular flow evaporation, most of the heat transfer degradation is a consequence of the use of the locally uniform equilibrium temperature in the measurements and calculation of the heat transfer coefficient. The remainder of the heat transfer degradation is due to nonlinear mixture property effects. The focus of the study was to determine the magnitude and the cause of the individual components of the heat transfer degradation of the studied mixtures.

The third study, A COMPARISON OF EXPERIMENTAL MEASUREMENTS OF LOCAL FLOW BOILING HEAT TRANSFER COEFFICIENTS FOR R11 AND R123, is presented in section 3 and presents a comparison of the measured horizontal, smooth-tube, flow boiling heat transfer coefficient of R11 to that of its proposed near ozone safe replacement, R123. The fluid properties of R11 and R123 are similar. The flow boiling data for the two fluids are similar for the convective region. However, the heat transfer coefficient for R11 in the nucleate flow boiling region was consistently observed to be, on average, 8.5% to

33% larger than that for R123. For the convenience of the reader, both the R123 and R11 property data used in this study are presented.

Acknowledgement

Section 1 of the work was funded jointly by NIST and EPRI RP 8006-2 under project manager Dr. Jong Kim. The authors would like to thank Dong Soo Jung, Michael Kauffeld, and Mark McLinden for their valuable inputs towards the completion of this work.

Section 2 of the work was funded jointly by NIST and DOE DE-AI01-91CE23808 under project manager Terry G. Statt. Additional funding was provided by EPRI RP 8006-2. The authors would also like to thank the following personnel of the NIST Thermophysics Division for their valuable inputs towards the completion of this work: Dr. M. O. McLinden, Dr. M. R. Moldover, Dr. G. Morrison, and Dr. D. Ripple.

Section 3 of the work was funded jointly by NIST and EPRI RP 8006-2 and RP 2792-09 under project managers Dr. Jong Kim and Dr. Powell Joyner, respectively. The authors would like to thank Dr. Graham Morrison for his valuable help in obtaining the R123 coefficients for the CSD equation of state. The authors would also like to thank Dr. Juergen Pannock, Mr. Peter Rothfleisch, Mr. Michael Kaul and Mr. Andrew Scott for their valuable contributions to this work.

CONTENTS

Section Page

1 VISUALIZATION OF NUCLEATE FLOW BOILING FOR AN R22/R114 MIXTURE AND ITS COMPONENTS 1-1

Introduction 1-1

Test Apparatus 1-4

Experimental Logic 1-7

Experimental Measurements 1-10

Calculations of Mass Quality 1-11

Experimental Results 1-13

Pure R114 at P_r=0.015 1-13

R22, R114, and Mixture at P_r=0.063 1-20

Conclusions 1-23

References 1-27

2 CAUSES OF THE APPARENT HEAT TRANSFER DEGRADATION FOR REFRIGERANT MIXTURES 2-1

Introduction 2-1

Experimental Work Investigated 2-10

Effect of Fluid Properties on $h_{2\phi}$ 2-15

Mixing Rules 2-15

The Less Volatile Components 2-18

Components of Degradation. 2-20

Circumferential and Radial Gradients. 2-26

Conclusions 2-31

References 2-34

3 A COMPARISON OF EXPERIMENTAL MEASUREMENTS OF LOCAL FLOW BOILING HEAT TRANSFER COEFFICIENTS FOR R11 AND R123 . . 3-1

Introduction 3-1

Test Apparatus 3-2

Properties of R123 3-4

Test Results 3-7

Detailed Discussion 3-7

Overview Discussion 3-17
Comparison of Data to Existing Correlations . . . 3-20
Conclusions 3-25
References 3-28

ILLUSTRATIONS

Section	Figure		Page
1	1-1	Schematic of the visualization test section	1-4
	1-2	Main test rig and visualization section	1-6
	1-3	Functional form of pool boiling given by Cooper[7]	1-9
	1-4	Flow boiling of R114 at P_r=0.015	1-14
	1-5	Measured bubble frequency for different qualities	1-15
	1-6	Measured bubble diameter for different qualities	1-16
	1-7	Heat load required to nucleate one bubble continuous for a particular quality	1-18
	1-8	Comparison of measured heat load to theory of Gungor and Winterton [9]	1-19
	1-9	Flow boiling for R114 and a mixture for x=0.01%. P_r=0.063	1-21
	1-10	Flow boiling for R114, R22, and a mixture for x=4%, P_r=0.063	1-22
	1-11	Flow boiling for R114, R22, and a mixture for x=7%, P_r=0.063	1-23
	1-12	Flow boiling for R114, R22, and a mixture for x=11%, P_r=0.063	1-24
	1-13	Flow boiling for R114, R22, and a mixture for x=14.4%, P_r=0.063	1-25
2	2-1	Phase equilibrium diagram for R22/R114 at P_r=0.08	2-2
	2-2	Phase equilibrium diagram for R12/R152a at P_r=0.08	2-3
	2-3	Phase equilibrium for R13B1/R152a at P_r=644 kPa	2-4

Section	Figure		Pages
2	2-4	Connection gradients within the liquid film	2-5
	2-5	Typical relationship of mixture flow boiling with respect to composition . . .	2-7
	2-6	Measured horizontal flow boiling heat transfer coefficients for the R13B1/R152a mixture (Ross et al.(1987))	2-11
	2-7	Measured horizontal flow boiling heat transfer coefficient for the R22/R114 mixture (Jung and Didion, 1989)	2-12
	2-8	Measured horizontal flow boiling heat transfer coefficient for the R12/R152a mixture (Jung and Didion, 1989)	2-13
	2-9	Impact of the mixing rule on the apparent heat transfer degradation of the R22/R114 mixture	2-17
	2-10	Effect of evaluating liquid properties at x_m and x_{ml} on $h_{2\phi}$	2-19
	2-11	Comparison of fluid property and concentration gradient effects on the degradation of R12/R152a heat transfer	2-21
	2-12	Comparison of fluid property, radial, and circumferential gradient effects on the degradation of R22/R114 heat transfer	2-22
	2-13	Effects of vapor-liquid composition difference on the heat transfer degradation	2-23
	2-14	Concentration difference versus liquid composition	2-26
	2-15	Measured circumferential liquid film concentration distributed for a 48% mole R22/R114 (Jung et al., 1989) .	2-28

Section	Figure		Pages
3	3-1	Schematic of Test Apparatus	3-2
	3-2	Comparison of h Versus x for R11 and R123 at Re = 18000 and q" = 20 kW/m^2	3-11
	3-3	Comparison of h Versus x for R11 and R123 at Re = 24000 and q" = 20 kW/m^2 . . .	3-12
	3-4	Effects of Reynolds Number on the Heat Transfer Quality Dependence for both R11 and R123	3-14
	3-5	Comparison of the Flow Boiling Characteristics of R11 to R123 for q" = 30 kW/m^2 and Re = 18000	3-15
	3-6	Comparison of h Versus x for R11 and R123 at q" = 30 kW/m^2 and Re = 24000	3-16
	3-7	Effect of Heat Flux on the Flow Boiling Characteristics of R11 and R123	3-17
	3-8	Comparison of Data to Existing Correlations	3-22

TABLES

Section	Table		Page
1	1-1	Fluid Properties at Test Conditions . .	1-26
3	3-1	CSD Eq. of State Coefficients for R123 and R11	3-7
	3-2	Thermodynamic Properties of R123	3-8
	3-3	Thermodynamic Properties of R11	3-9
	3-4	Actual Heat Transfer Parameter for Data	3-10
	3-5	Effects of Heat Flux on Heat Transfer Coefficient	3-18
	3-6	Effect of Reynolds Number on Heat Transfer	3-19
	3-7	Comparison of Heat Transfer of R11 to that of R123	3-19
	3-8	Percent Over-prediction of R11 Data by Correlations	3-23
	3-9	Percent Over-prediction of R123 Data by Correlations	3-24

Nomenclature

English Symbols

a	coefficients of CSD equation of state
b	coefficients of CSD equation of state
Bo	Boiling number, $q''\pi D_i^2/(4\dot{m}\ddot{a})$
c	coefficients of ideal gas heat capacity
Co	Convection number, $((1-x)/x)^{0.8}\ (\rho_v/\rho_l)^{0.5}$
C_p	specific heat of liquid (kJ/kg K)
D_b	maximum bubble diameter (m)
D_i	internal tube diameter (m)
E_c	percent overprediction of data for $x < 0.13$
E_n	percent overprediction of data for $x > 0.13$
f_b	bubble frequency (1/s)
F_l	fluid factor in eq. 8
F	enhancement factor in eq. 7
h	horizontal flow boiling heat transfer coefficient (W/m^2-K)
h_i	$h_{2\phi}$ from linear interpolation of single components (W/m^2-K)
h_l	single phase, all liquid, heat transfer coefficient (W/m^2-K)
h_n	pool boiling heat transfer coefficient in eq. 7 (W/m^2-K)
h_p	$h_{2\phi}$ predicted using single component correlation (W/m^2-K)
$h_{2\phi}$	two-phase heat transfer coefficient (W/m^2-K)
i	refrigerant enthalpy (kJ/kg)
k	thermal conductivity (W/m-K)
L	length (m)
$\dot{m}$	mass flow rate (kg/s)
L_N	number of frames for growth and release of bubble
N_f	nucleate factor in eq. 7
P	absolute pressure (Pa)
P_c	critical pressure (Pa)
P_r	reduced pressure, P/P_c

q''	heat flux (W/m^2)
G	mass flux (kg/m^2-s)
q	heat spent on vaporization (W)
q_b	latent heat required to generate one bubble (W)
q_c	convective boiling heat load (W)
q_e	Heat imposed with copper strip on quartz tube (W)
q_n	normalized heat load
q_p	heat load obtained from electrical heating (W)
q_s	heat load spent on subcooled heating (W)
q_∞	heat load from surroundings (W)
r	coordinate perpendicular to heat transfer surface (m)
Re	Reynolds number, $\rho_l u D_i/\mu_l$
S	steady state film speed (frames/s)
T	temperature (K)
T_{in}	temperature of refrigerant entering main test rig (K)
T_c	critical temperature (K)
T_r	reduced temperature, T/T_c
T_s	saturation temperature of refrigerant (K)
T_{wi}	internal wall temperature (K)
T_i	temperature of liquid-vapor interface (K)
T_s	saturated fluid temperature (K)
T_w	inside tube wall temperature (K)
UA	overall heat conductance (W/K)
u	average liquid velocity (m/s)
V_b	volume of vapor generated per unit time (m^3/s)
x	mole fraction of more volatile component
x_m	mass fraction of more volatile component
x_q	thermodynamic quality
x_t	transition quality
y	coordinate along heated surface (m)
z	coordinate along tube axis (m)

Greek symbols

$\Delta h_{2\phi}$	$h_i - h_{2\phi}$ (W/m^2-K)
λ	latent heat of vaporization (kJ/kg)
ρ_l	density of liquid (kg/m^3)
ρ_v	density of vapor (kg/m^3)
ρ	density (kg/m^3)
ρ_{exp}	experimentally measured density (kg/m^3)
μ	dynamic viscosity (kg/m-s)

Subscripts

b	bottom of tube
c	critical
l	liquid
m	mixture or mass
s	saturation state
t	top of tube
v	vapor
1	component number one
2	component number two

Section 1

VISUALIZATION OF NUCLEATE FLOW BOILING FOR AN R22/R114 MIXTURE AND ITS COMPONENTS

Introduction

Investigators have found that phase change by means of bubble nucleation is more efficient for a single liquid component than it is for a mixture of two or more liquids [1,2,3]. Heat transfer coefficients for pool boiling of multi-component mixtures, where the growth of bubbles at a solid-liquid interface is the main heat transfer mechanism, are in general lower than those of the individual components [3]. Depending on the quality, both bubble nucleation and interface evaporation can be important in the boiling of a flowing fluid within a horizontal tube. Jung [4] has found that heat transfer coefficients for flow boiling of refrigerant mixtures inside horizontal tubes are lower than those which would be obtained from an ideal mixing rule between the pure components (and sometimes even lower than either component). His study revealed that the degradation of the binary mixture heat transfer was present for qualities from 10 to 90%. In general, the deviation of mixture heat transfer coefficients from an ideal mixing rule were shown to increase for decreasing quality. In other words, the deviation of the heat transfer from an ideal mixing rule was greatest for the nucleate boiling regime. Thus, one is led to believe that the cause of the heat transfer degradation with low quality is associated with bubble nucleation or growth.

Nucleate boiling can also be reduced or suppressed by a reduction in the average temperature of the liquid surrounding the bubble. Reduction of liquid superheat in flow boiling can be caused by an increase in the quality and/or mass velocity of the flow. Collier and Pulling [6] developed one of the first models to predict the

suppression of nucleate boiling during forced convection for single component fluids. Jung [4] suggested a suppression of nucleate boiling with increasing quality for refrigerants and refrigerant mixtures. His single component data for $\dot{m}$ = 0.033 kg/s, q" = 36 kW/m^2, and P_r = 0.08 has shown that bubble growth ceases at 47% quality for R114. His data for R22, for the same P_r and q" as the R114 data but different $\dot{m}$, ($\dot{m}$ = 0.045 kg/s), show that bubble suppression occurs at 25% quality. Also, nucleate boiling for a mixture that was a 48%R22/52%R114 ($\dot{m}$ = 0.033 kg/s, q" = 36 kW/m^2, and P_r = 0.08) was suppressed at 26% quality, which is nearly the value at which pure R22 was suppressed. These data suggest a nonlinear relationship between the composition and the quality at which suppression occurs.

Further investigations into the flow boiling of refrigerants, which has been relatively neglected as compared to that of water, are necessary in order to fully understand the phenomena. For example, flow boiling heat transfer water data of Kenning and Hewitt [5] has shown that the heat transfer coefficient is relatively independent of quality for the nucleate boiling region. Conversely, Jung [4] has shown that the flow boiling heat transfer coefficient for refrigerants is strongly dependent on the quality for the same nucleate boiling region. The difference is probably due to the relatively low thermal conductivity of the refrigerant as compared to that of water, but this can not be known for certain without further investigation.

There is not sufficient understanding of nucleate boiling of multi-component mixtures to develop a model to predict such a phenomenon. The criterion most commonly used to determine if suppression has occurred is to examine the heat transfer data for lack of heat flux dependence. Although, this seems to be based on sound rationale, there still exists a large degree of uncertainty since this criteria is derived from pressure, temperature and mass flow

measurements - not from visual observation. The nucleate boiling contribution to total heat transfer is obtained by subtracting what is thought to be the convective portion from the total. Thus, both the nucleate boiling and the convective boiling portions are obtained by indirect measurement.

This article presents a case study of nucleate flow boiling. The results presented here are by no means useful in the design of evaporators. That is, neither heat transfer coefficients nor wall superheats are presented. Instead, visual results that characterize the mechanisms of nucleate flow boiling are presented. It is intended that the characterization of the boiling will stimulate thought on the measurement and the cause of the fundamental mechanisms that govern the heat transfer. The first objective of this study is to become familiar with the difficulties associated with obtaining detailed bubble measurements and what is required to overcome these problems. Three sections of this paper deal with situations encountered and remedies revealed in the experimental logic, and measurements methods. The second objective of this study is to visually demonstrate the suppression of nucleate boiling with increasing quality for flow boiling within a horizontal tube. The visual demonstration of suppression is useful since it verifies that suppression does occur and it is also useful since the relationship between suppression and quality can be experimentally quantified. Future studies may establish a comparison between suppression for refrigerants and other fluids, e.g. water. The third objective is to compare the relative activity of nucleate flow boiling for the R22/R114 mixture of arbitrary composition to that for the single components R22 and R114 for the same heat flux and flow conditions. The resulting data has been used to demonstrate the relative differences between bubble generation in binary mixtures and that in single component refrigerants. Also, the data can be used to determine if the bubble activity of the flowing mixtures is degraded in a similar magnitude as for mixtures in pool boiling experiments.

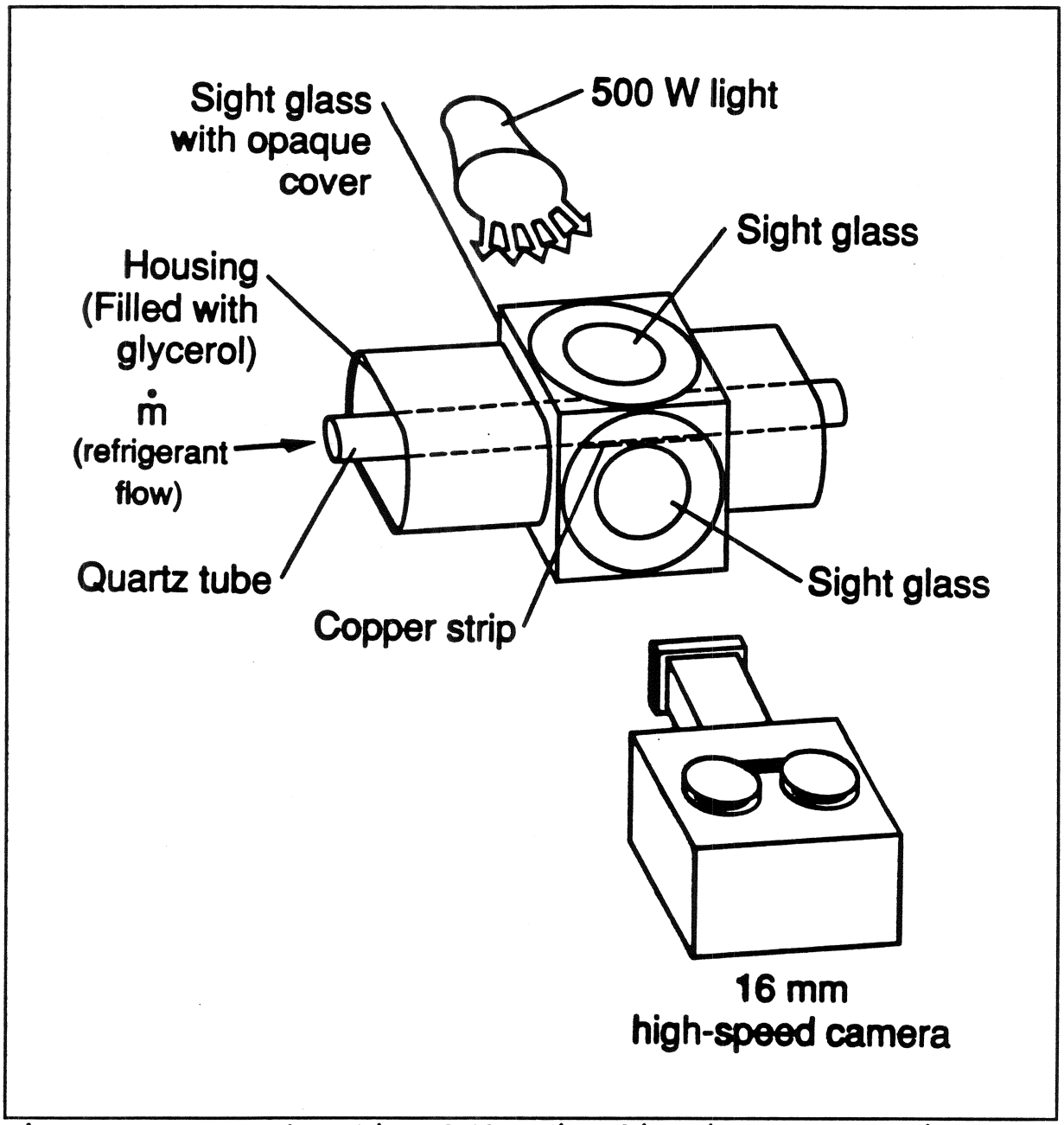

Figure 1-1 Schematic of the visualization test section.

Test Apparatus

Figure 1-1 shows a schematic of the visualization test section. The 9 mm i.d., quartz tube was enclosed in a housing as shown. The space between the inside of the housing and the outside of the tube

was filled with glycerol to limit reflections from the tube which would have otherwise caused poor photographic images. A 16mm high speed camera was used to make motion picture films of the flow boiling process within the horizontal quartz tube. The camera was positioned in front of the sight glass so that the plane of the view was parallel to the direction of flow. Figure 1-1 also shows that a 500 W concentrated light source was placed in front of another sight glass opposite of the camera to produce a back lighting configuration. An translucent cover was placed between the light and the sight glass to give uniform illumination of the quartz tube. The inside of the quartz tube was polished with a 5 micron abrasive to create a surface which is similar to the inside of stainless steel tubing. Similarity of the quartz roughness to the steel roughness was verified by visual inspection with an electron microscope. The roughened surface would ensure active cavity nucleation. The quartz tube was electrically heated by a 4 mm wide copper strip placed along the bottom of the outside of the tube. The localized heat flux produced nucleation only at the bottom of the tube. Bubble growth on the sides and top of the tube was not present. This ensured an unobstructed view of bubble growth on the bottom of the tube.

The main test rig, shown in Figure 1-2, was used by Jung in his work. A more detailed discussion of it can be found in his thesis [4]. The main test rig was used to set the mass flow rate and the entering quality to the visualization section. Figure 2 shows that the test rig consists of two 4 m lengths of 9.1 mm i.d., .25 mm wall thickness 304 stainless steel tube connected by a u-bend. The tubing was heated by a D.C. voltage which produced a constant heat flux boundary condition. The test fluid was pumped through the inside of the tube and increased in quality as it boiled along the length until it reached the condenser where it was condensed and returned to the pump. Measured tube wall temperatures and fluid pressures of the main test rig were used to calculate the quality at the entrance to the visualization section. A detailed

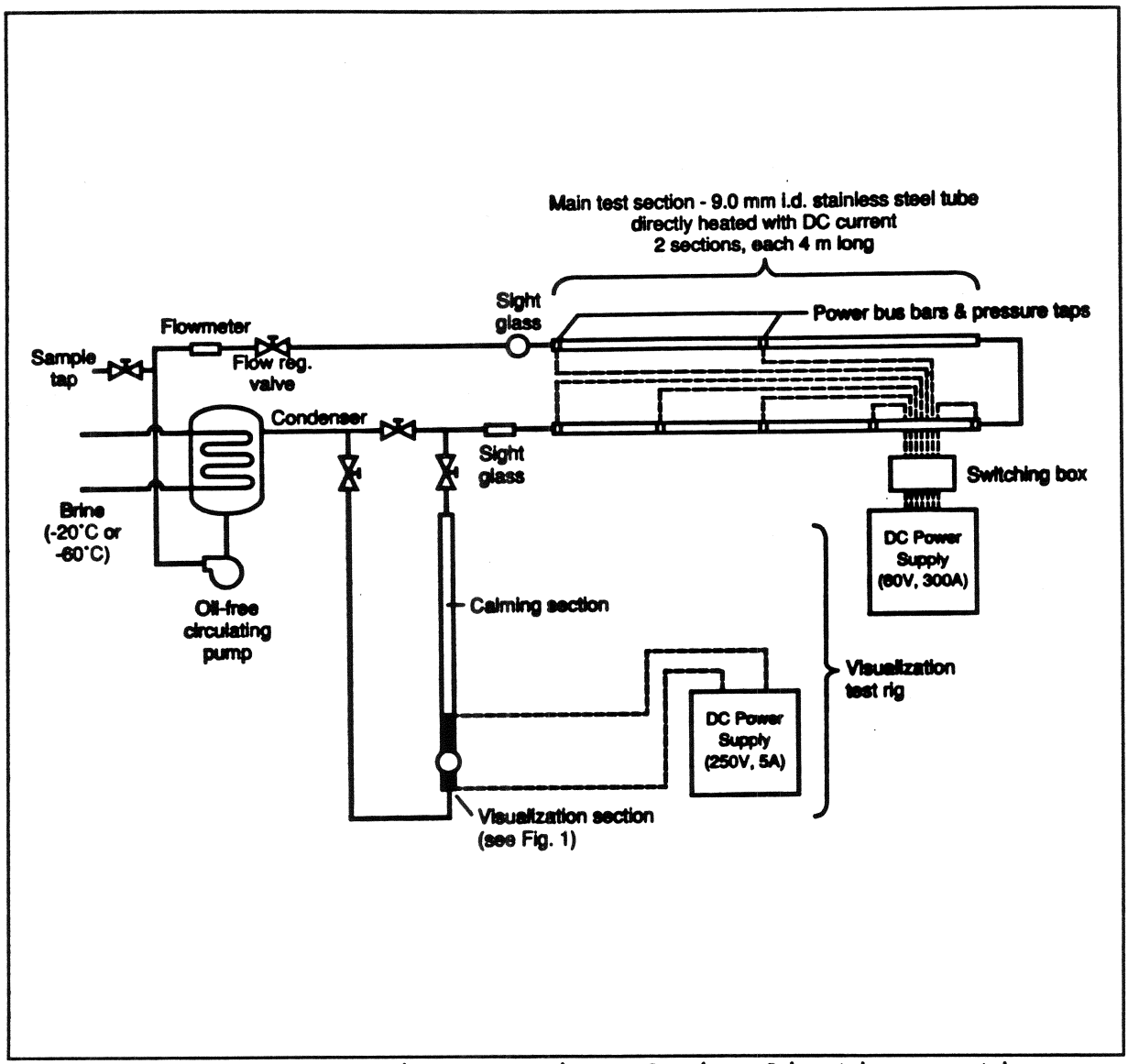

Figure 1-2 Main test rig and visualization section

discussion of the calculation of the quality is given in a later section.

Figure 2 shows that a 2 m calming section was used to connect the visualization test section to the main test rig. This length is not electrically heated, but it receives a marginal amount of heat from the surroundings (not enough to cause nucleation). The calming section allows most of the remaining bubbles from the main

test rig to combine with the main vapor slug so that these bubbles will not be attributed as being generated in the quartz tube. This ensures that only those bubbles generated in the quartz tube will be photographed and analyzed.

Experimental Logic

This section outlines the logic used in choosing the thermodynamic conditions at which the tests were conducted. The final operating condition was dictated by the lower temperature limit of the test rig.

The first step was choosing the operating parameters which would be fixed while varying quality and fluid. From examination of correlations [1,4,5,6], it was felt that the refrigerant total mass flow rate ($\dot{m}$) and the heat flux (q") to the quartz tube were strong functions of heat transfer and should be held constant for all tests. The authors also felt that the fluid pressure should be chosen as the remaining fixed operating condition. Cooper [7] has shown that, for most fluids, nucleate boiling on the outside of horizontal cylinders is proportional to the following form involving only reduced pressure (P_r):

$$\frac{h}{(q'')^{0.69}} \propto P_r^{0.056}(-\log_{10} P_r)^{-0.7} \qquad (1\text{-}1)$$

Equation 1 shows that the heat transfer by nucleation has the same functional form regardless of the fluid. Thus, the magnitude of nucleate boiling for different fluids should differ only by a constant. Consequently, as Equation 1 suggests, comparisons of the data for the different fluids were made at equal P_r. The next step was to determine the P_r at which to operate the tests.

Two criteria were used to choose the pressure at which the tests were conducted. First, the pressure had to be below the structural limitations of the test rig. Second, in order to make direct

measurement of bubble growth, it was essential that an unobstructed view of the bubble was attained. Equation 1 implies that nucleate boiling measurements taken at low reduced pressure will have fewer active sites. Individual bubbles are less likely to be disturbed by other bubbles for low P_r boiling since there is less interaction between bubbles. Thus, it was possible to examine a single bubble and directly measure the bubble diameter and frequency for R114 data at $P_r = 0.015$. After consideration of the structural limitation and the desired visual conditions, a low reduced pressure was chosen for test. The final step was to determine the magnitude of P_r for test.

Figure 1-3 is a plot of the right side of Equation 1 versus P_r. Figure 3 shows that the nucleate boiling potential sharply increases with P_r for $P_r < 0.05$ and for $P_r > 0.8$, and is comparatively flat for $0.05 < P_r < 0.8$. This demonstrates that measurements taken in the $0.05 < P_r < 0.8$ region would be less sensitive to the inaccuracies of the pressure measurement. However, preliminary tests with R114 showed the number of active sites present for $0.05 < P_r < 0.8$ prohibited the examination of the growth of a single bubble. The tests were finally conducted at the lowest possible P_r which was attainable in the test rig, which was $P_r = 0.015$ for R114. At this pressure, examination of individual bubble growth was possible for R114.

Attempts were made to take data for all fluids at $P_r = 0.015$. Unfortunately, the lowest temperature limit of the existing test rig was not sufficient to attain $P_r = 0.015$ for R22 and the mixture. The lowest possible P_r attainable in the test rig for R22 and the mixture was $P_r = 0.063$. The consequence of taking data at $P_r = 0.063$ can be examined with the aid of Equation 1. Figure 1-3 shows that there is a 62% increase in the nucleate boiling potential from $P_r = 0.015$ to $P_r = 0.063$. The investigators found that indeed there were many more bubbles present at $P_r = 0.063$ than

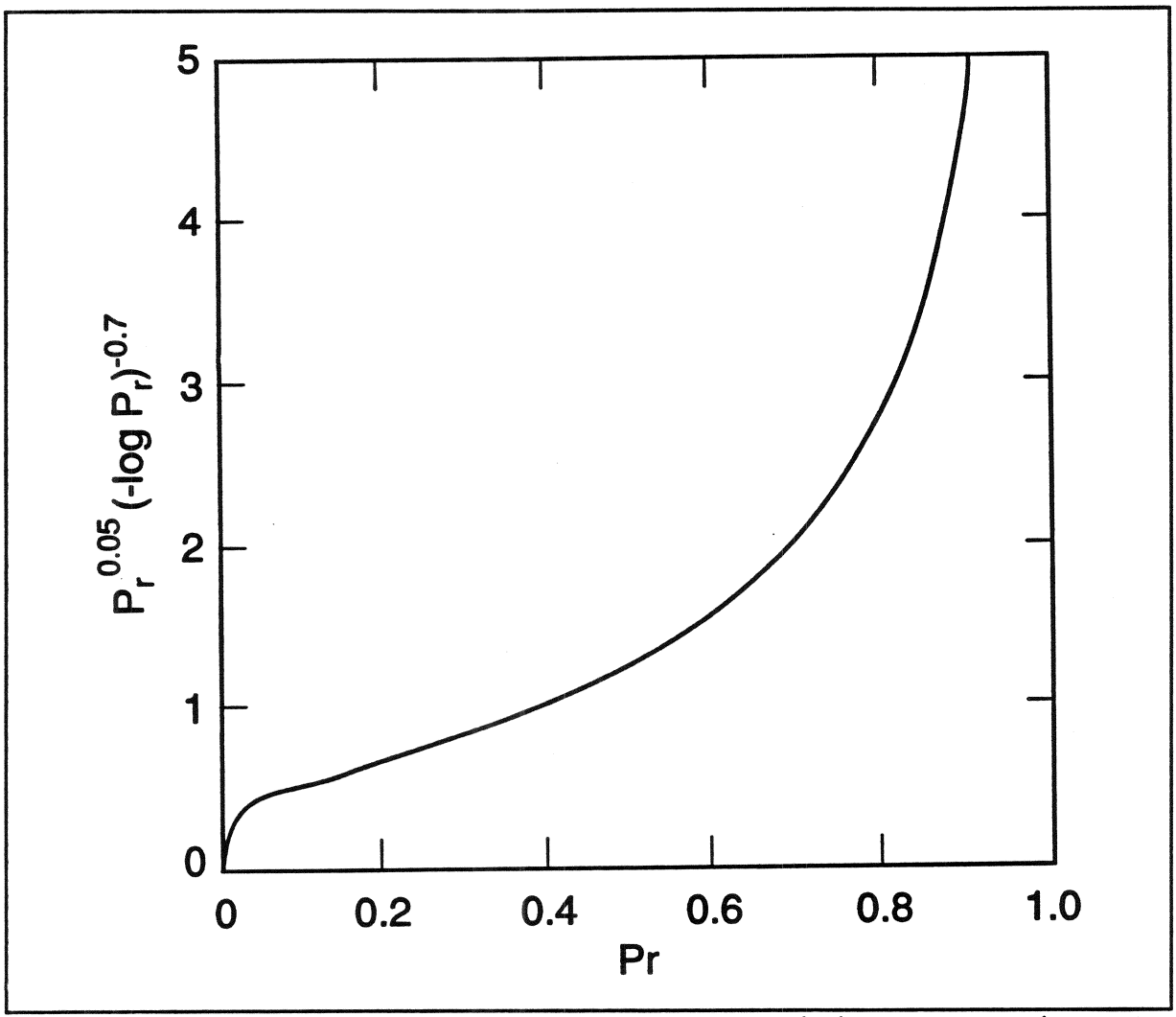

Figure 1-3 Functional form of pool boiling data given by Cooper [7].

there were at P_r = 0.015 for R114. Detailed measurement of bubble parameters was not possible at P_r = 0.063 due to the frequent interaction of bubbles. As a result, the data at high P_r was analyzed subjectively. Because the data sets were analyzed differently, the experimental results were discussed separately as high and low P_r conditions. The refrigerants 22, 114 and the mixture were all examined at P_r = 0.063, which is referred to here as the high P_r condition. Only R114 was examined at P_r = 0.015 (low P_r).

Experimental Measurements

The bubble frequency and the bubble size can both be measured at low reduced pressures. The bubble frequency, f_b, was obtained by counting the number of motion picture frames (N_f) from the growth to the release of the bubble from the solid-liquid interface and dividing into the steady state film speed (S), i.e.:

$$f_b = \frac{S}{N_f} \tag{1-2}$$

Care was taken to ensure that measurements were made only when the film speed had reached 7000 frames/s. Timing marks on the film were used for this purpose. The bubble departure diameter (D_b) was the maximum diameter of the bubble obtained just after departure from the wall-liquid interface. The bubble diameter was obtained by measuring both the bubble diameter and the quartz tube diameter from the film and scaling down to obtain D_b from the known quartz tube diameter. The bubble geometry was approximated as spherical for the calculation of the amount of vapor contained in the bubble. Efforts were made to measure the bubble size soon after departure from the wall and also when it appeared to be most spherical. The volume of vapor generated for a single bubble per unit time (V_b) was calculated as:

$$V_b = \frac{f_b \, \pi \, D_b^3}{6} \tag{1-3}$$

From V_b, the latent portion of the heat load required to generate one bubble (q_b) is:

$$q_b = \lambda \rho_v V_b \tag{1-4}$$

The accuracy of equation 1-4 is not calculable. The calculation relies on the ability to quantify the deviation of the bubble shape from spherical. If the uncertainty in the shape of the bubble can

be represented as an error in the measurement of D_b, then a 10% error in the measurement of D_b will cause a 30% error in the calculation of V_b and consequently, cause a 30% error in the calculation of q_b. Although the accuracy of q_b is unknown, it is felt that since the experimental procedure was consistent for all the data, the q_b can be used to successfully investigate trends.

High pressure data (P_r = 0.06-0.065) at a mass flow rate of 0.032 kg/s and a quartz tube heat flux of 64 kW/m^2 was taken for R22, R114 and the R22/R114 mixture. At this pressure, individual bubbles could not be isolated for study due to vigorous interaction with other bubbles. The temperature of the brine that was supplied to the condenser of the main test rig was not low enough to operate at lower pressures for R22 and the mixture. Consequently, the comparison of bubble nucleation for the different liquids remains mostly visual and subjective.

Calculations of Mass Quality

This section discusses the procedure used to calculate the quality (x) at the entrance to the visualization test section. Mass quality (x) is defined as the fraction of the total mass flow which is vapor:

$$x = \frac{\dot{m}_v}{\dot{m}} = \frac{q}{\dot{m}\lambda} \qquad (1\text{-}5)$$

The total mass flow rate ($\dot{m}$) is measured at the subcooled entrance to the main test rig with a calibrated turbine meter. The latent heat of vaporization (λ) is obtained from an equation of state for refrigerants and refrigerant mixtures derived by Morrison and McLinden [8]. The heat available for boiling (q) is a sum of that which is obtained from electrical heating in the main test rig (q_p) and obtained from the surroundings (q_∞) minus the heat required to bring the entering subcooled liquid to saturation (q_s), i.e.:

$$q = q_p + q_\infty - q_s \qquad (1\text{-}6)$$

The q_∞ is obtained from a calibrated UA and the temperature difference between the room and the average fluid temperature is measured for the 2 m calming section. The q_s was calculated as $\dot{m}$ Cp (T_s - T_{in}), where T_s is the saturation temperature of the refrigerant, and T_{in} is the temperature of the subcooled liquid entering the main test rig.

The gain in temperature due to viscous heating was calculated to be less than 0.1 K for all tests. The calculated qualities below 5% have an uncertainty of approximately ±12% for 99.7% confidence. The quality calculations in the range of 9-20% quality have an uncertainty of approximately ±5% for 99.7% confidence.

A visual method for calculating the quality using a photographic estimate of the void fraction and calculated density was also conducted. The uncertainty of the visual method was approximately ±20%. Consequently, this method was used only as a check on the calculation of the quality given by Equations 5 and 6. The quality calculated from Equations 5 and 6 was within the scatter of the quality obtained by the visual method.

Experimental Results

Pure R114 at P_r = 0.015

The following is a discussion of the experimental results of the convective, nucleate boiling of R114 at P_r = 0.015. Measurements of f_b, and D_b were done only for pure R114.

Figure 1-4 shows photographs taken from the high speed films for R114 at P_r = 0.015. The film number and the refrigerant number are located on the upper tube wall of the photographs. The dark area along the bottom of the quartz tube is the copper strip used to electrically heat the fluid. The main liquid-vapor interface of the flow is the dark, wavy line approximately 1/3 of a tube diameter up from the tube bottom. The vapor slug is above the liquid-vapor interface, and the liquid film is below the liquid-vapor interface. The vapor slug was surrounded by liquid for all qualities. The vapor bubbles are shown to be within the liquid and carried from the wall from left to right of the photograph.

Figure 1-4 shows that approximately ten different sites were visible along the 15 mm quartz tube length. Not all sites were present for all qualities. For example, the majority of sites were active at the lowest quality (x = 0.012) and only one site was active at the highest quality (x = 0.116), clearly demonstrating suppression of bubble growth at increased quality. However, some sites that were active at say x = 0.063 were not active at x = 0.012. Hence, these sites are not sufficient to demonstrate suppression due to quality increase. Only two sites were active for all qualities except the highest quality. Consequently, only the data of these two sites for R114 at P_r = 0.015 are discussed below. The authors feel that the f_b and D_b of the reported two sites measured at a given quality are representative of the f_b and D_b observed at the same quality for sites not reported.

Figure 1-5 shows the variation of the measured bubble frequency

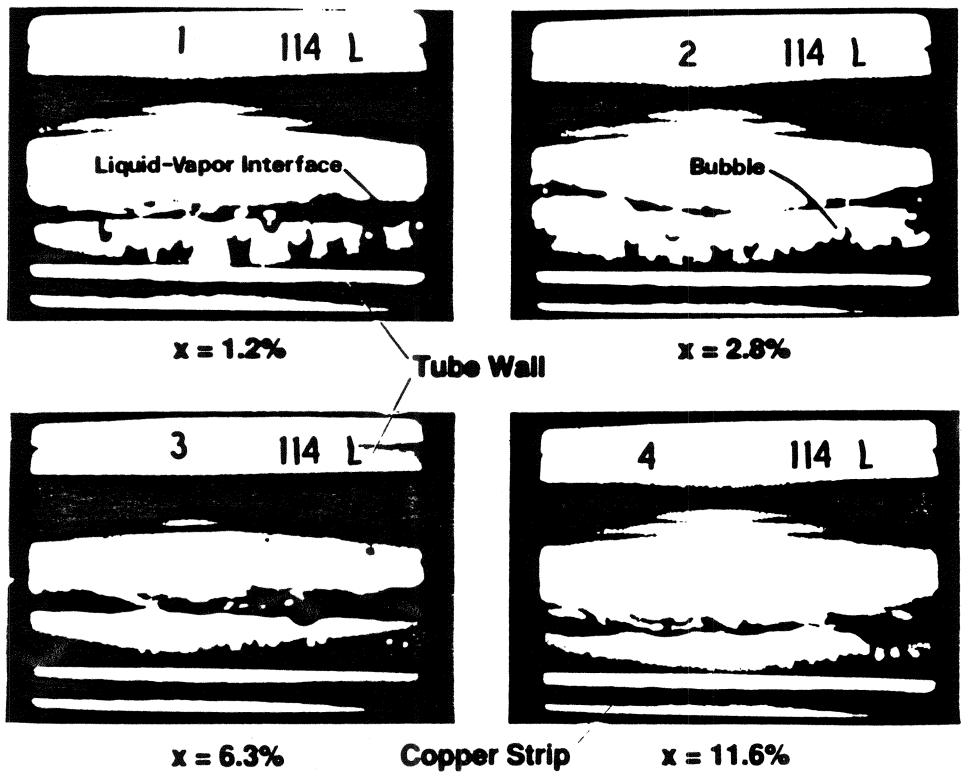

Figure 1-4 Flow boiling of R114 at P_r = 0.015.

(f_b) with quality (x) for two different nucleation sites; • and o. The f_b was obtained by averaging the frequency of five consecutive bubbles originating from the same site. One standard deviation for the measurement trials was approximately 16% of the measurement and is represented as an error bar for a data point of Figure 5. The large standard deviations are due to local changes in the flow conditions which are characteristic of chaotic flows. It is difficult to extract a functional relationship from the data with such a large standard deviation which is compounded with a small

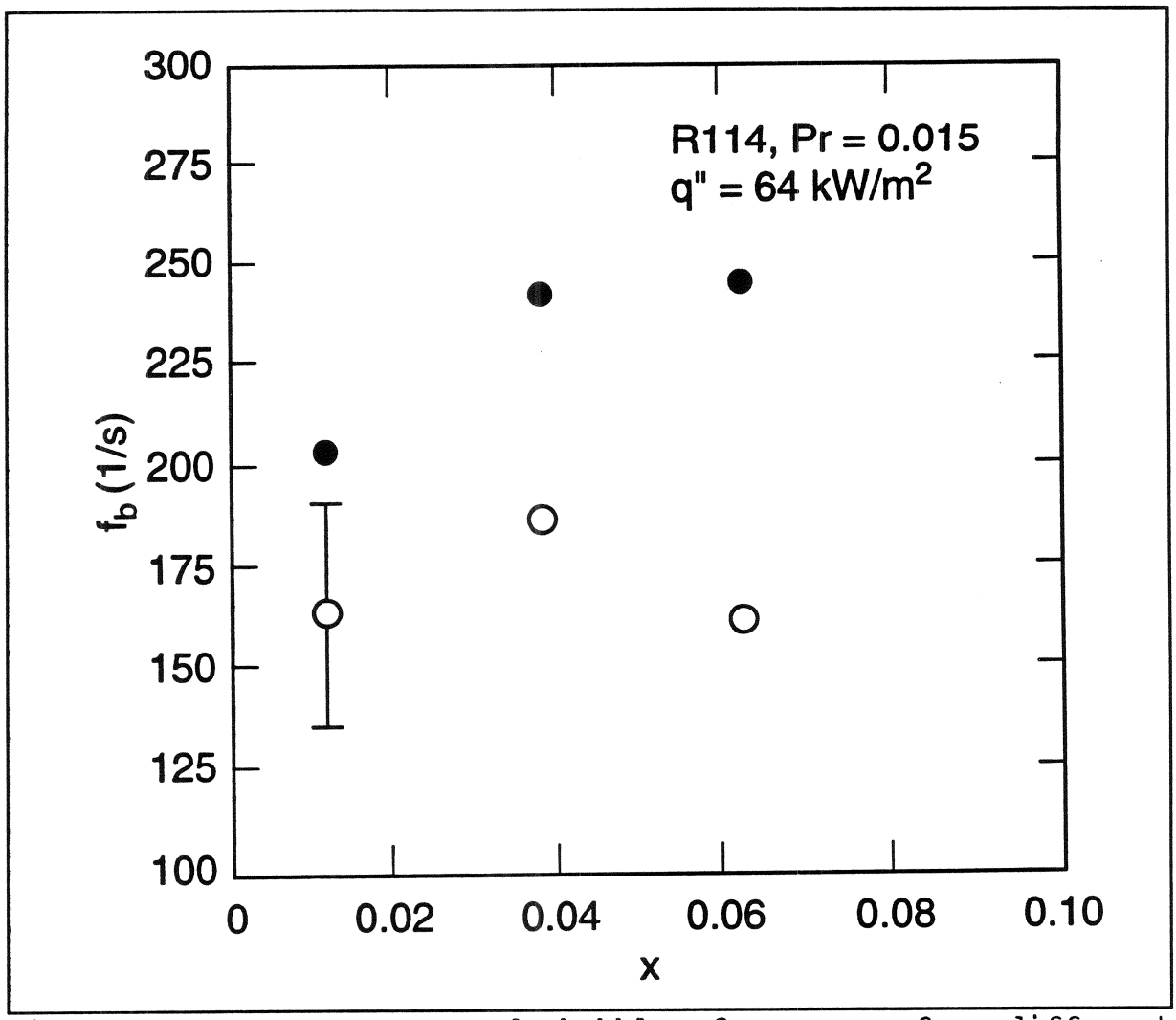

Figure 1-5 Measured bubble frequency for different qualities

change in the average f_b with quality. Consequently, no generalizations about the variation of f_b can be safely made. It is possible that the bubble frequency is coupled with quality and the wall temperature profile which is continually disturbed by the growth and release of adjacent bubbles. Clearly, more work must be done towards the establishment of a measurement method for f_b that will produce statistically sound data.

Figure 1-6 is a plot of the measured bubble diameter (D_b) versus

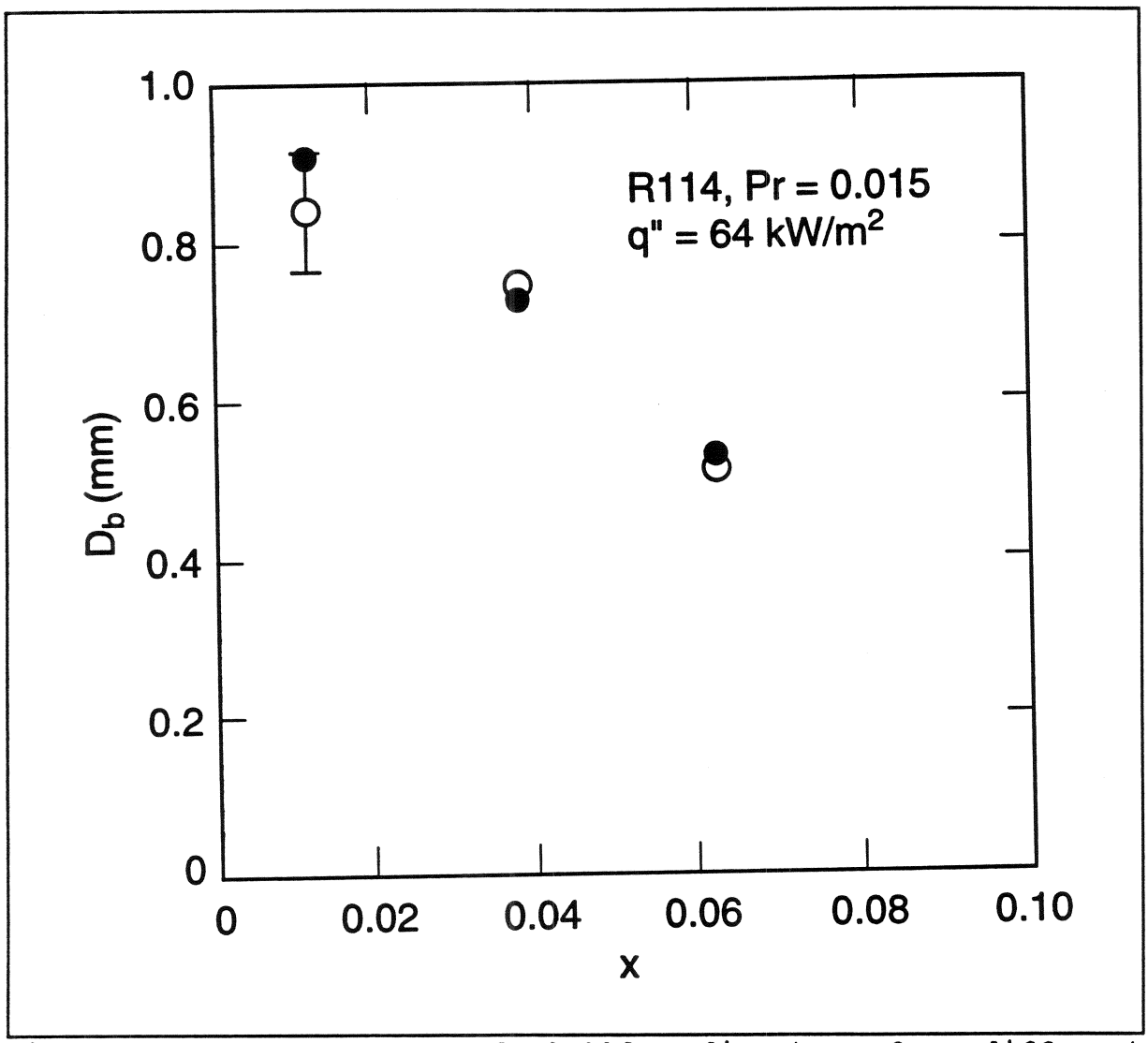

Figure 1-6 Measured bubble diameter for different qualities

quality. The standard deviation of the measured bubble diameter is relatively small and the change of D_b with quality is significant. Hence, the plot suggests a relatively linear relation between decreasing bubble diameter and increasing quality. This is not to say that this relation is appropriate for all boiling surfaces, fluids and flow conditions. The purpose here is to merely suggest that the measurement of the bubble diameter from high speed film can produce successful results.

The heat imposed with the electrically heated copper strip (q_e) onto the bottom of the quartz tube is dissipated by two very different mechanisms. The first mechanism is nucleate boiling. Nucleate boiling requires a superheated liquid layer and sites from which bubbles can grow. The focus of measurements in this paper is on the latent component of nucleate boiling (q_b), i.e, only the heat for phase change and not the energy for superheating the liquid. The heat that is not used to nucleate is conducted and convected through the liquid film to the liquid-vapor interface where it is convected and evaporated away by the vapor phase. This second mechanism is called convective evaporation (q_c) in this paper. The first resistance to convective evaporation is the liquid film on the tube wall. Low thermally conductive liquids (like refrigerants), thick films (low qualities) and small velocities (low mass flow rates) all contribute to the resistance to q_c. The resistance to q_c decreases for increasing quality due to smaller liquid film thickness and higher liquid and vapor velocities associated with high qualities. Consequently, the fraction of q_e which is q_c increases for increasing quality. The fraction of q_e which is q_b correspondingly decreases for increasing quality.

Equation 1-4 was used along with the measured f_b and D_b to calculate the heat load required to generate one vapor bubble (q_b) and plotted versus quality in Figure 1-7. Figure 1-7 demonstrates, as discussed above, that q_b decreases with increasing quality for fixed total mass flow rate and fixed imposed heat flux. The lower q_b is a result of higher vapor velocities which reduce the thermal resistance to q_c, thus removing superheat from the wall. Although the standard deviation is approximately 25% of the plotted q_b, the q_b is convincingly shown to decrease with increasing quality.
Figure 1-8 is a plot of the heat required for nucleation of R114 at $q'' = 64\ kW/m^2$ during flow boiling normalized by the heat required for nucleation evaluated at $x = 0.012$. Data obtained from the

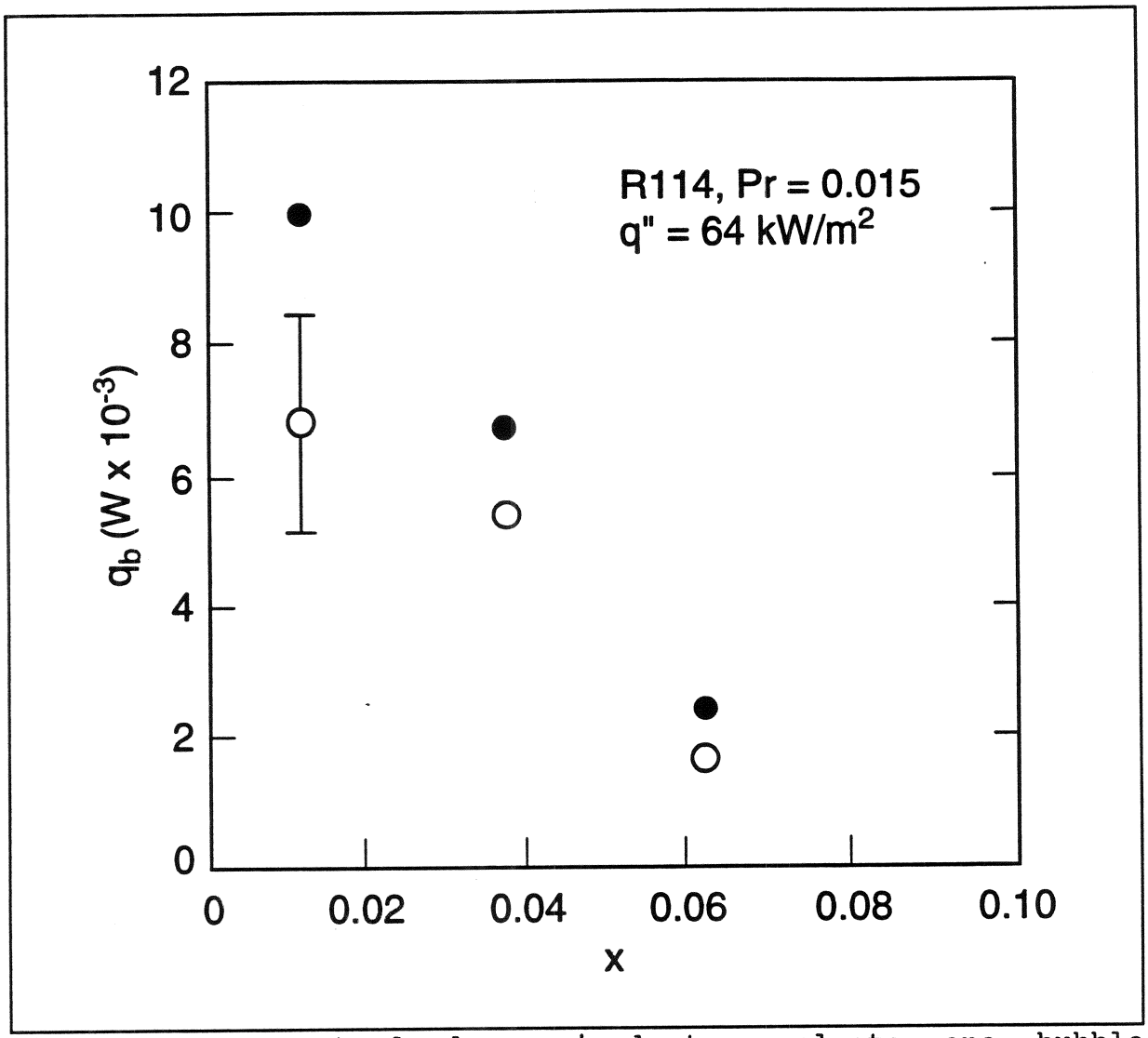

Figure 1-7 Heat load required to nucleate one bubble continuously for a particular quality.

films are plotted for two different sites. The data for these two sites agree well with each other, demonstrating the trend of decreased vapor generation with increased quality. The nucleate boiling portion of a flow boiling correlation by Gungor and Winterton [9] is plotted as a solid line on this graph. Gungor and Winterton modified Cooper's [10] pool boiling correlation with their own suppression factor to obtain an expression for the nucleate portion of a correlation for flow boiling within a horizontal tube. The nucleate portion of the correlation and data

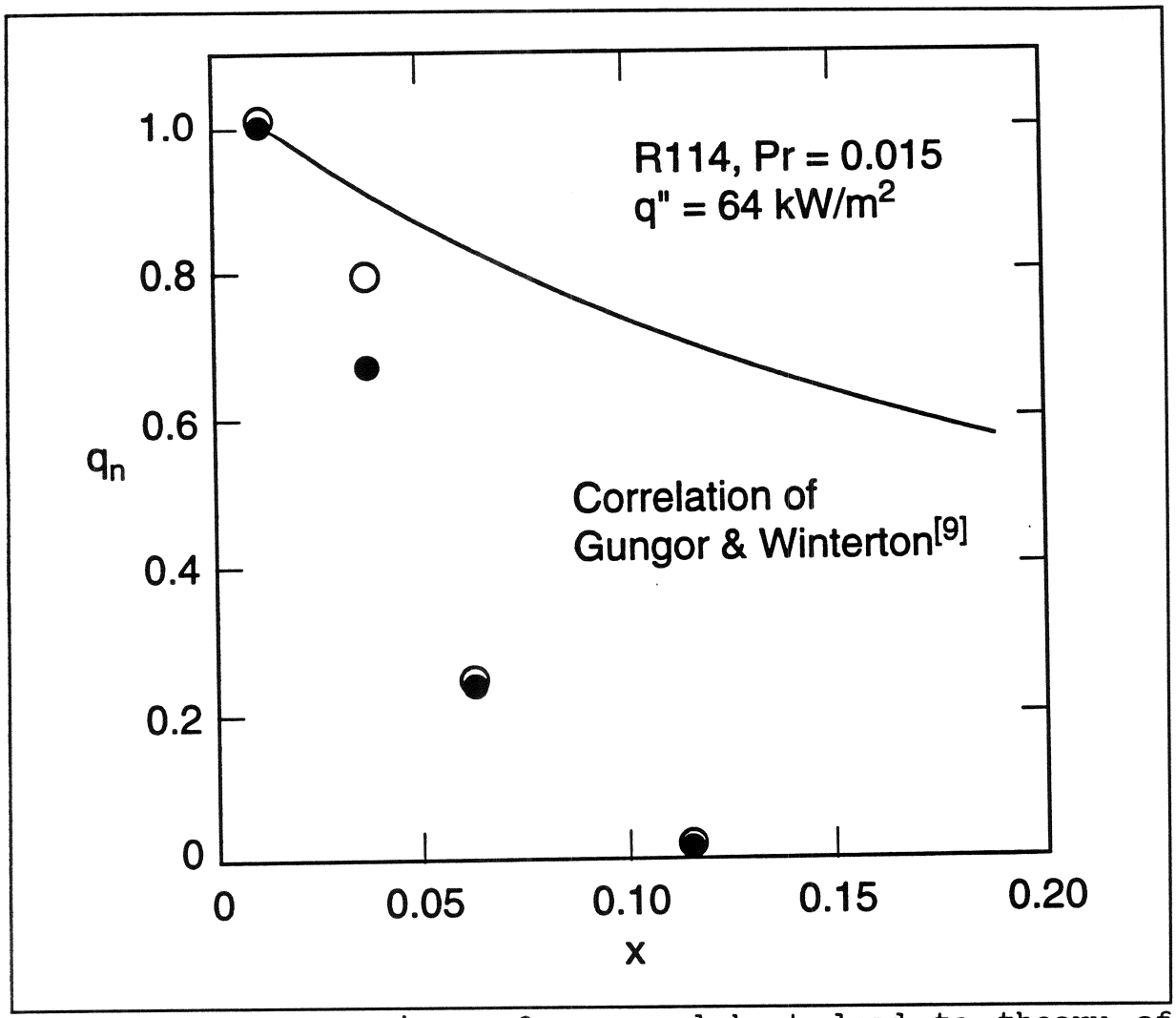

Figure 1-8 Comparison of measured heat load to theory of Gungor and Winterton [9].

depart for the higher qualities. For example, the correlation predicts only a 23% reduction from the amount of nucleation at x = 0.012 to x = .11, whereas the data show, no bubbles are generated at x = .11 for sites • and o.

The discrepancy between the data and Gungor and Winterton's correlation can be partially attributed to a difference between measured surface roughness of the quartz tube and the surface roughness assumed for the correlation. Gungor and Winterton [9]

assumed that the surface roughness of the tube was 1 μm. The surface roughness of the quartz tube was estimated from an electron microscope to be 0.5 - 0.2 μm. The smaller cavities of the quartz tube result in less heat transfer by bubble nucleation than what would be expected from a larger, 1 μm cavity. Another cause for the difference between the data and theory may be inability of the Gungor and Winterton correlation to predict the suppression factor for the data. Their suppression factor is calculated from a simple and convenient correlation which relies on very few fluid properties. Consequently, it is understandable how the simple correlation for the suppression factor may not predict the suppression trends for the particular data set presented here.

R22, R114 and mixture at P_r = 0.063

The remaining data will be examined solely by photographic evidence. Figures 1-9 through 1-13 are photographs taken from the high speed films for R114, R22 and the 37.7% mole R22/62.3% mole 0R114 mixture all at P_r = 0.061. Immediately, three general observations can be obtained from the figures. First, the number of bubbles present decreases as quality increases for all fluids studied. Second, for a given quality, R114 exhibits more bubbles than either R22 or the mixture. Third, the amount of nucleation by R22 and the mixture seems to be approximately the same. This is true even though the liquid mixture is mostly R114 by mole fraction. One might assume that the bubble activity ought to be a mole weighted activity where the resulting bubble activity would more closely resemble that of R114. The visual observations contradict this premise.

Table 1-1 shows the fluid properties at the test conditions for all of the fluids tested. The last column of Table 1-1 represents the volume of vapor generated per joule of energy for a single bubble ($1/(\lambda\ \rho_v)$). The volume of vapor can be equated with the activity of nucleation. Likewise, the per unit energy can be equated to the

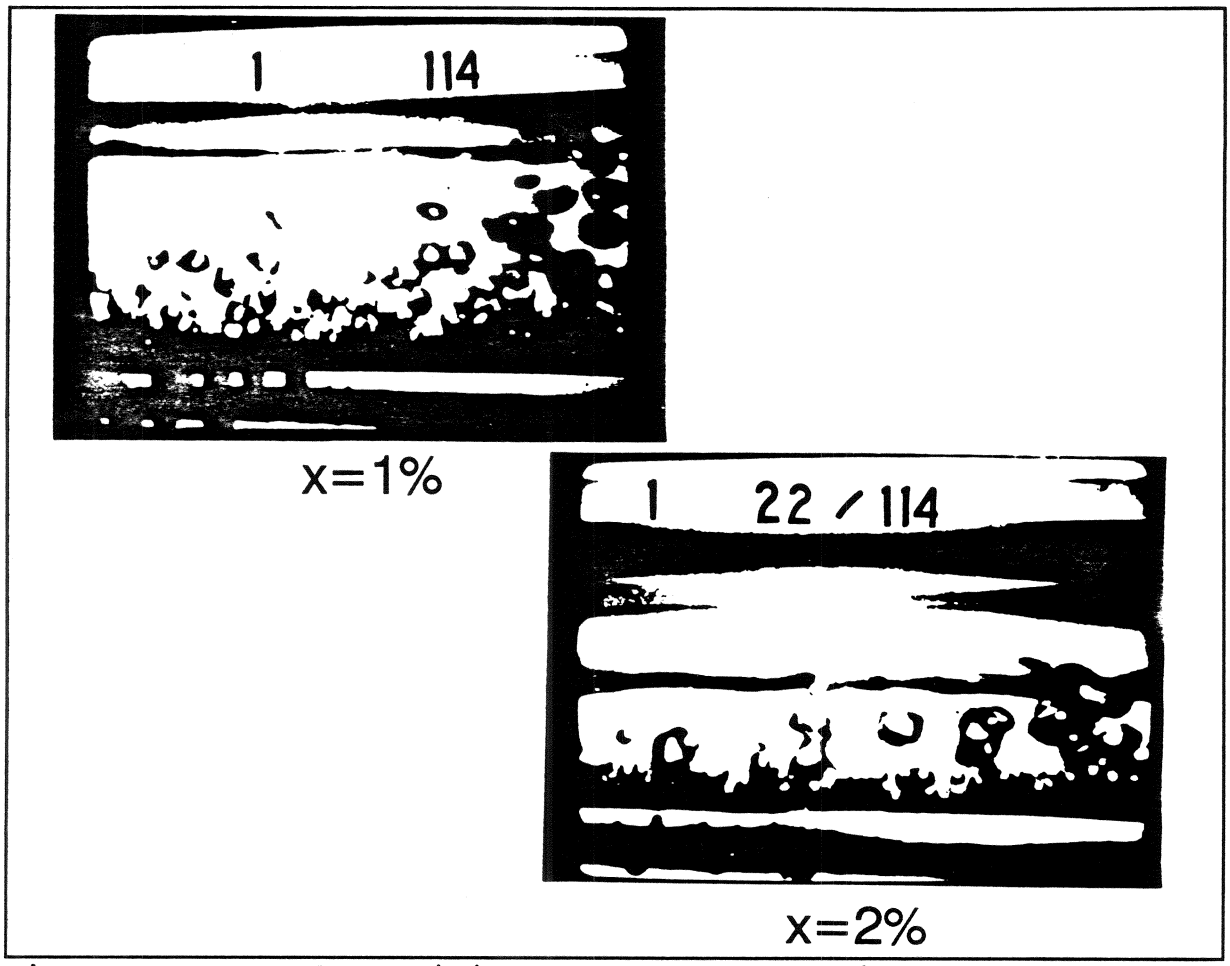

Figure 1-9 Flow boiling for R114 and a mixture for near x = 0.01, P_r = 0.063.

last column of Table 1-1 shows that, for fixed heat flux, the predicted volume of vapor generated, or nucleate activity, for R22 differs by only 8% from that for the mixture. This suggests that the amount of nucleation for R22 should not differ much from the mixture. This is supported by the photographs in Figures 10 through 12. Notice also that $1/(\lambda\ \rho_v)$ for R114 is 42% larger than $1/(\lambda\ \rho_v)$ for R22. The photographic evidence also supports this significant difference between the nucleate boiling for R114 and R22.

Another factor that determines the nucleate flow boiling activity

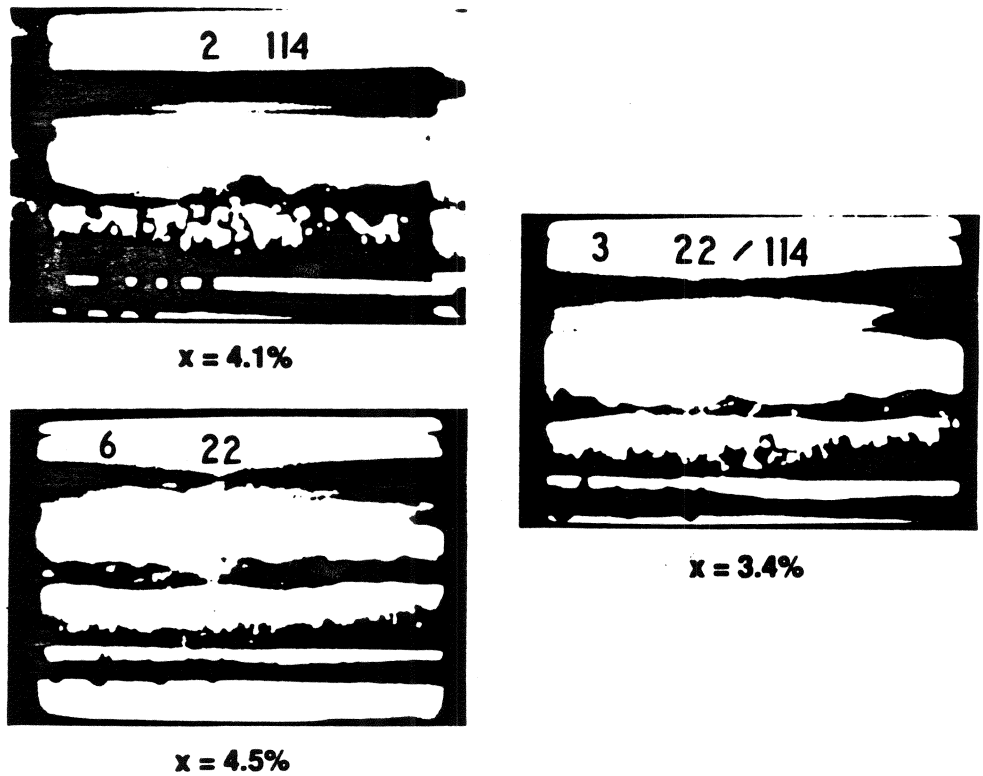

Figure 1-10 Flow boiling for R114, R22, and a mixture for x = 0.063

of a liquid is its thermal conductivity (k_l). If it was possible to have a fluid that would become less thermally conductive for fixed flow and heat transfer conditions, it would be possible to observe a corresponding loss in bubble activity due to increased convection. Superheat is more readily convected from the wall for fluids with higher k_l. Consequently, nucleate flow boiling, in response to reduced wall superheat, will become less vigorous. The fifth column of Table 1 demonstrates the trend of liquids with lower thermal conductivity to exhibit more nucleate activity. For example, k_l of R114 is 41% lower than that for R22; this agrees with the result of this paper which indicates that the volume of

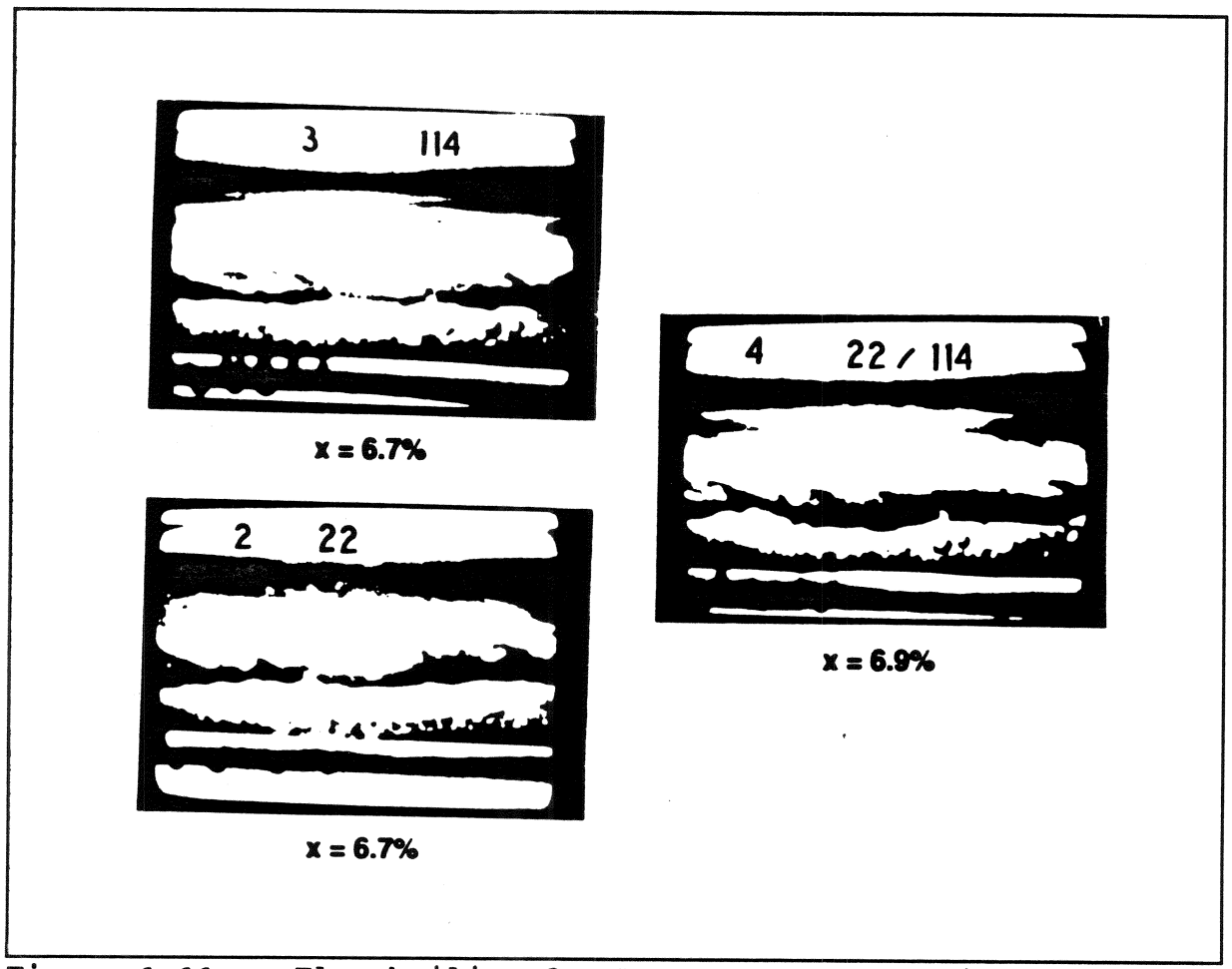

Figure 1-11 Flow boiling for R114, R22, and a mixture for x = 7%, P_r = 0.063

vapor generated with R114 was greater than that of R22 for the same P_r. The thermal conductivity of the R114 is increased by 21% by the addition of R22 to obtain a 37.3% mole mixture. The thermal conductivity of the liquid has been raised and the bubble activity correspondingly drops.

Conclusions

It has been visually demonstrated that a decrease in nucleate boiling during flow boiling is associated with an increase in quality for R114, R22 and a 37.7%R22/62.3%R114 mixture. The reduction in nucleate activity was demonstrated for the heat flux, total mass flow rate, and the reduced pressure-all fixed.

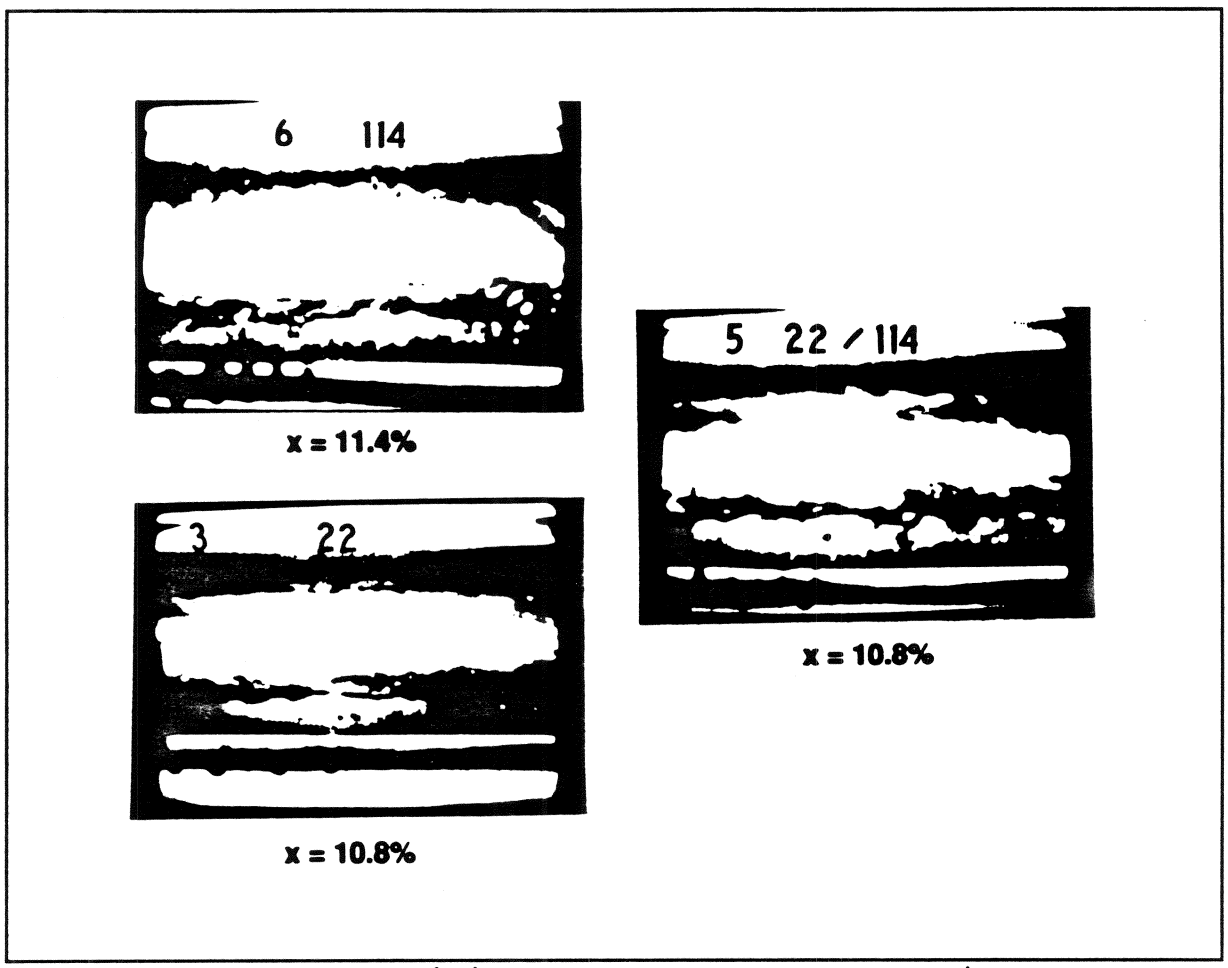

Figure 1-12 Flow boiling for R114, R22, and a mixture for x = 7%, P_r = 0.063.

Nucleation activity was shown to be also suppressed by a reduction in fluid pressure which is in agreement with the trend of Cooper's [7] correlation for pool boiling on the outside of a horizontal cylinder. The films suggest that for a given quality R114 exhibits much more nucleation than either R22 or the mixture. The amount of nucleation demonstrated by R22 and the mixture was comparable even though the mixture was mostly R114 by mole. Arguments using the latent heat of vaporization, the vapor density and the liquid thermal conductivity have been made to explain the visual trends.

This study has shown that the parameters essential to obtaining the

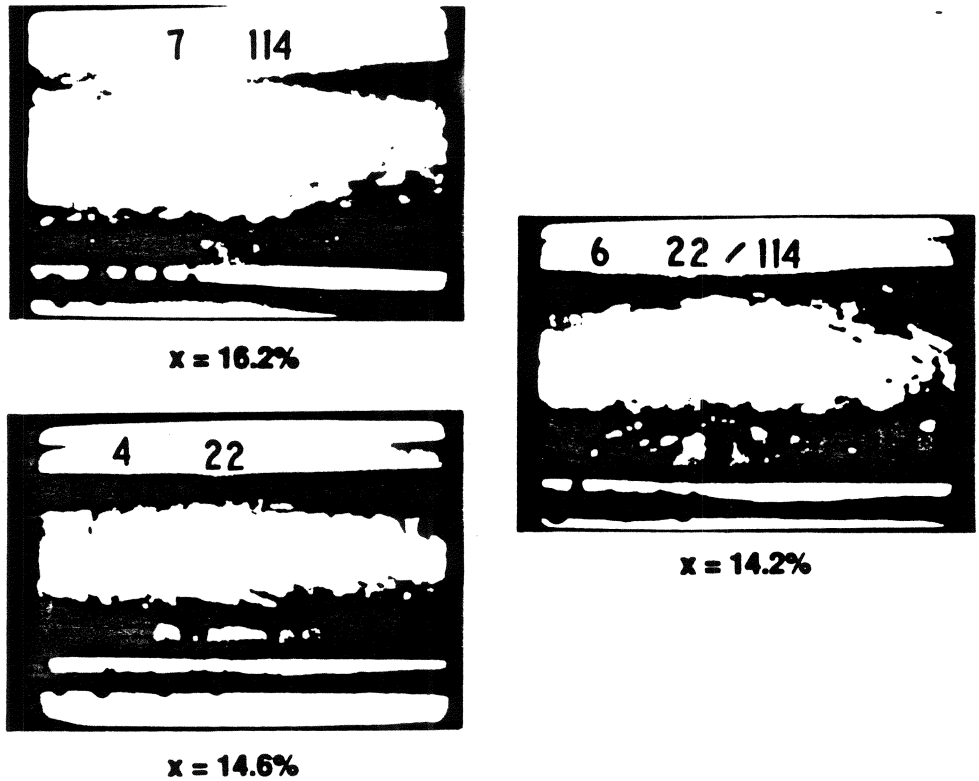

Figure 1-13 Flow boiling for R114, and R22, and a mixture for $x = 14.4\%$, $P_r = 0.063$

heat required for the growth and release of a bubble can be measured directly at low reduced pressure. However, there still remain some difficulties associated with the precision of the frequency measurement. Specifically, the measured bubble frequency had a large standard deviation and did not show a consistent tendency with quality. Further investigation is required to develop a method that can be used to produce statistically sound bubble frequency measurements. On the other hand, the bubble diameter was shown to be amenable to measurement by the high speed film technique as demonstrated by the low standard deviation of the measurement and consistent trends of the measurement with quality.

Table 1-1: Fluid Properties at Test Conditions

Fluid	T_s (K)	P_s (kPa)	λ (J/kg)	k_1 (W/m K)	g/mol	ρ_v (kg/m^3)	$1/\lambda\rho_v$ [(m^3/J)x10^{-7}]
R114	297	206	126.947	0.0647	170.92	15.95	4.94
R22	259	305	216.373	0.1068	86.47	13.31	3.47
R22/R114	271	265	160.834	0.0825	139.08	16.41	3.79

References

1. D. Gorenflo, P. Blein, G. Herres, W. Rott, H. Schomann and P. Sokol, "Heat Transfer at Pool Boiling of Mixtures with R22 and R114," Int. J. Refrig., Vol. 11, July 1988, pp. 257-263.

2. T. O. Hui and J. R. Thome, "A Study of Binary Mixture Boiling: Boiling Site Density and Subcooled Heat Transfer," Int. J. Heat Mass Transfer, Vol. 28, No. 5, 1985, pp. 919-928.

3. K. Stephan,"Heat Transfer in Boiling of Mixtures", Proc. 2nd. Heat Transfer Conf. 7th Munich, 1982, pp. 59-81.

4. D. S. Jung,"Mixture Effects on Horizontal Convective Boiling Heat Transfer", Ph.D. thesis, University of Maryland, 1987.

5. D. B. R. Kenning and G. F. Hewitt, "Boiling Heat Transfer in The Annular Flow Regime," 8th IHTC, San Francisco, 1986, pp. 2185-2190.

6. J. G. Collier and D. J. Pulling,"Heat Transfer to two-phase gas-liquid systems. Part II: Further data on steam/water mixtures in the liquid dispersed region in an annulus", AERE-R 3809, 1962.

7. M. G. Cooper, "Correlations for Nucleate Boiling - Formulation Using Reduced Properties," PhysicoChem Hydrodynamics, Vol. 3, no. 2, 1982, pp. 89-111.

8. G. Morrison and M. O. McLinden, "Application of a Hard Sphere Equation of State to Refrigerants and Refrigerant Mixtures," NBS Technical Note 1226, NBS, Gaithersburg, MD, 1986.

9. K. E. Gungor and R. H. S. Winterton, "A General Correlation for Flow Boiling in Tubes and Annuli," Int. J. Heat and Mass Transfer, Vol. 29, No. 3, pp. 351-358, 1986.

10. M. G. Cooper, "Saturation Nucleate Pool Boiling. A Simple Correlation, "1st U.K. National Conference on Heat Transfer, Vol. 2, pp.785-793,(I.Chem.E. Symposium Series No. 86,1984).

Section 2

CAUSES OF THE APPARENT HEAT TRANSFER DEGRADATION FOR THE REFRIGERANT MIXTURES

Introduction

Pool boiling of mixtures has been practiced since antiquity. The ancient Greeks made their drinking water by distilling sea water. In the 19th century oil was refined by distillation to make kerosene for lamps. Although the practical application of mixture heat transfer is very old, the experimental and theoretical study of it is relatively new. The study of in-tube flow boiling of refrigerant mixtures is especially recent. During this short period of study, researchers have found that liquid mixtures do not evaporate as efficiently as single component liquids. However, mixtures of refrigerants can be used to enhance the efficiency of refrigeration equipment as compared to single component refrigerants [1]. Unfortunately, the decrease or degradation in the efficiency of the evaporation of mixtures increases the costs of the performance improvements that can be achieved by using mixtures in cycles. This study is an attempt to further the understanding of horizontal flow boiling of mixtures with the hope of generating ideas that might lead to reduction of the heat transfer degradation associated with refrigerant mixtures.

There are two fundamental thermodynamic differences between single component fluids and mixtures which, in turn, cause fundamental differences between the phase change characteristics of single component fluids and mixtures. First, at constant pressure, the mixture temperature rises during evaporation, while the temperature of the single component fluids remains constant. Second, the liquid and vapor compositions are different in the mixture, while they are identical in the single component. These points are demonstrated by the phase equilibrium diagrams for the three binary mixtures investigated here, viz., R22/R114, R12/R152a, and R13B1/R152a which are shown in Figs. 2-1 through 2-3, respectively.

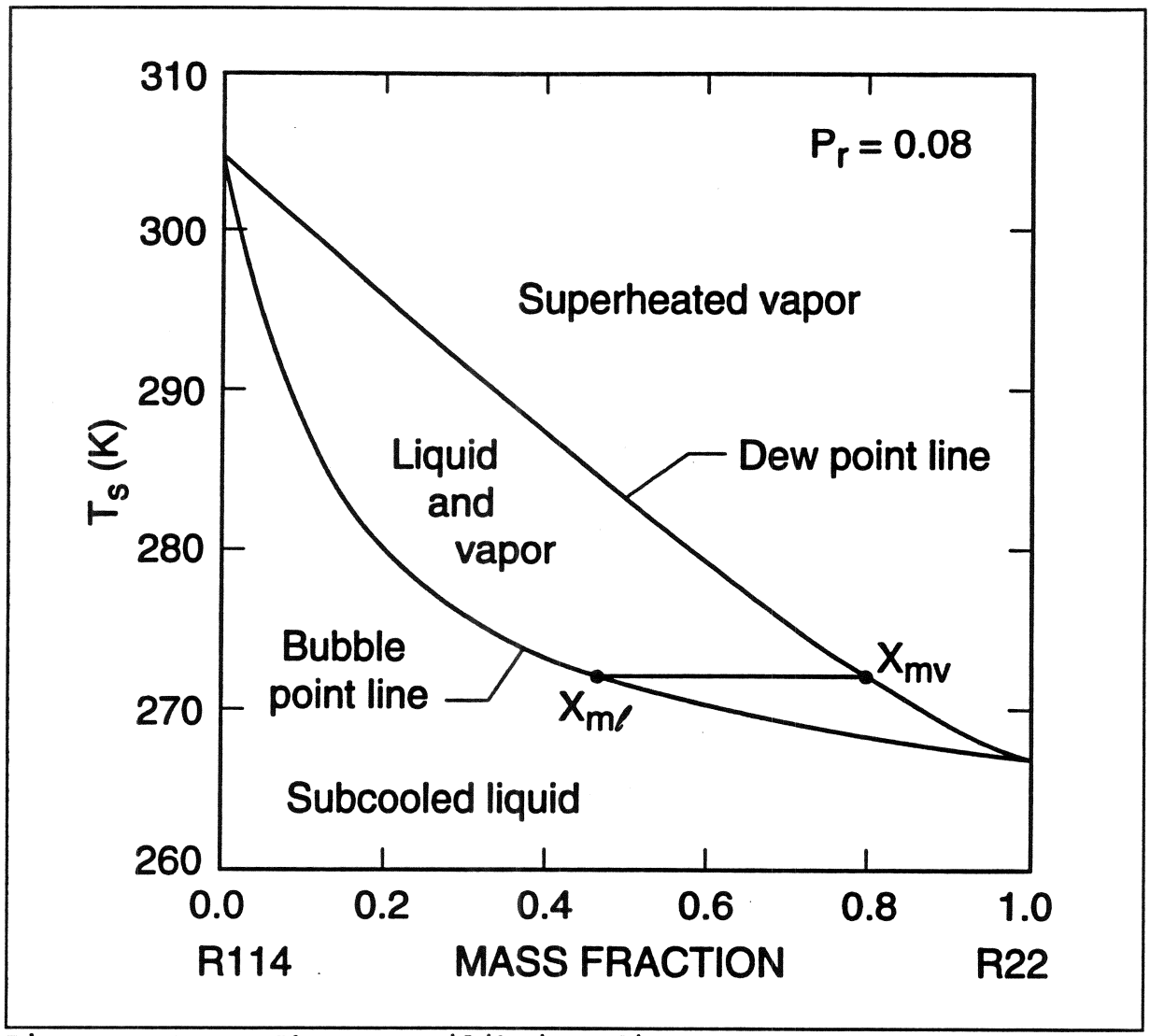

Figure 2-1 Phase equilibrium diagram for R22/R114 at P_r = 0.08

Figure 2-1, the phase equilibrium diagram for the R22/R114 mixture at a reduced pressure (P_r) of 0.08, represents the thermodynamic state of the mixture at equilibrium conditions. The phase equilibrium diagram is a plot of equilibrium temperatures versus the mass fraction of the more volatile component. The more volatile component is R22, since its equilibrium or saturation temperature is lower than that of R114 at the same pressure. The lower line is the bubble point line. It represents the variation

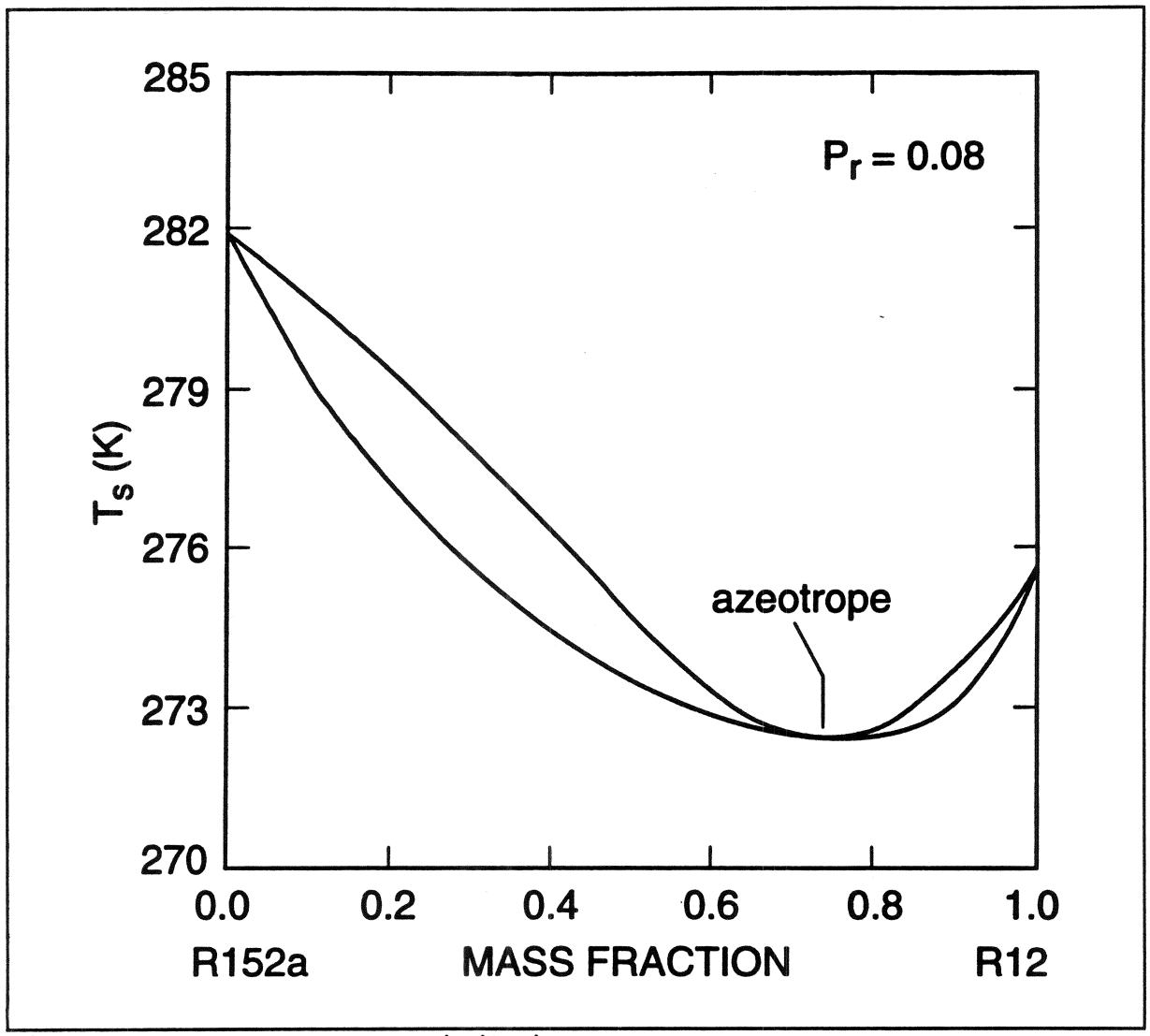

Figure 2-2 Phase equilibrium for R12/R152a at P_r = 0.08

of the liquid saturation temperature with composition. The upper line is the dew point line, and it represents the variation of the saturated vapor temperature with composition. The area between the dew point and bubble point lines represents a two-phase mixture with a liquid of composition x_{ml} and a vapor of composition x_{mv} in coexistence. The vertical distance between the dew point and bubble point lines, i.e., the temperature glide, may loosely be used to determine the potential for the heat transfer degradation of a particular mixture. The heat transfer of a binary mixture,

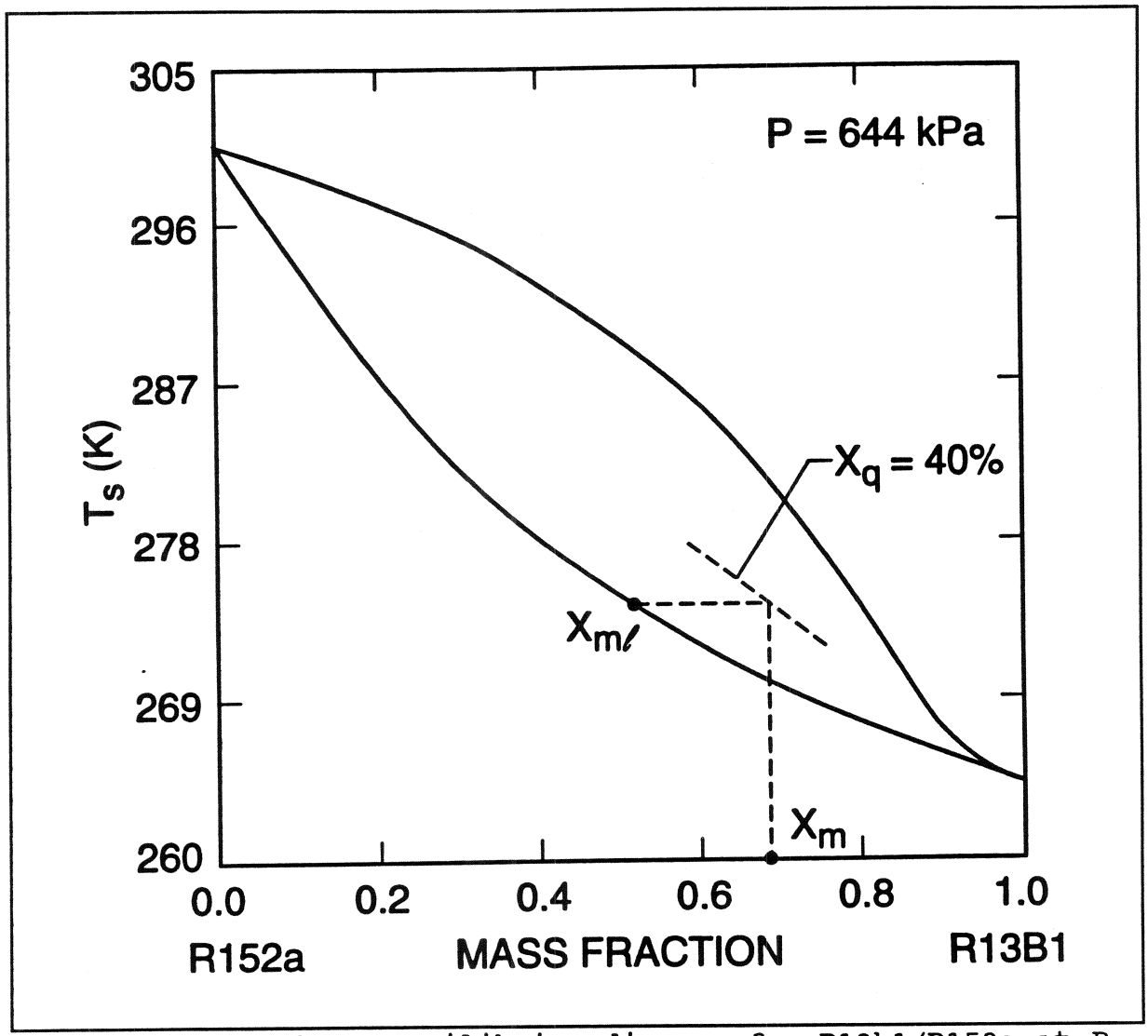

Figure 2-3 Phase equilibrium diagram for R13b1/R152a at P = 644 kPa

which has a large temperature glide, is likely to be lessened by concentration gradients. Correspondingly, an azeotrope, which is a mixture that has no temperature glide, is likely to exhibit very little heat transfer degradation. Figure 2-2 shows that an azeotrope exists at x_m = 0.738 R12, as depicted by the tangency of the dew and bubble lines.

Figure 2-4 illustrates the concentration gradients that are established within a liquid mixture film as a consequence of

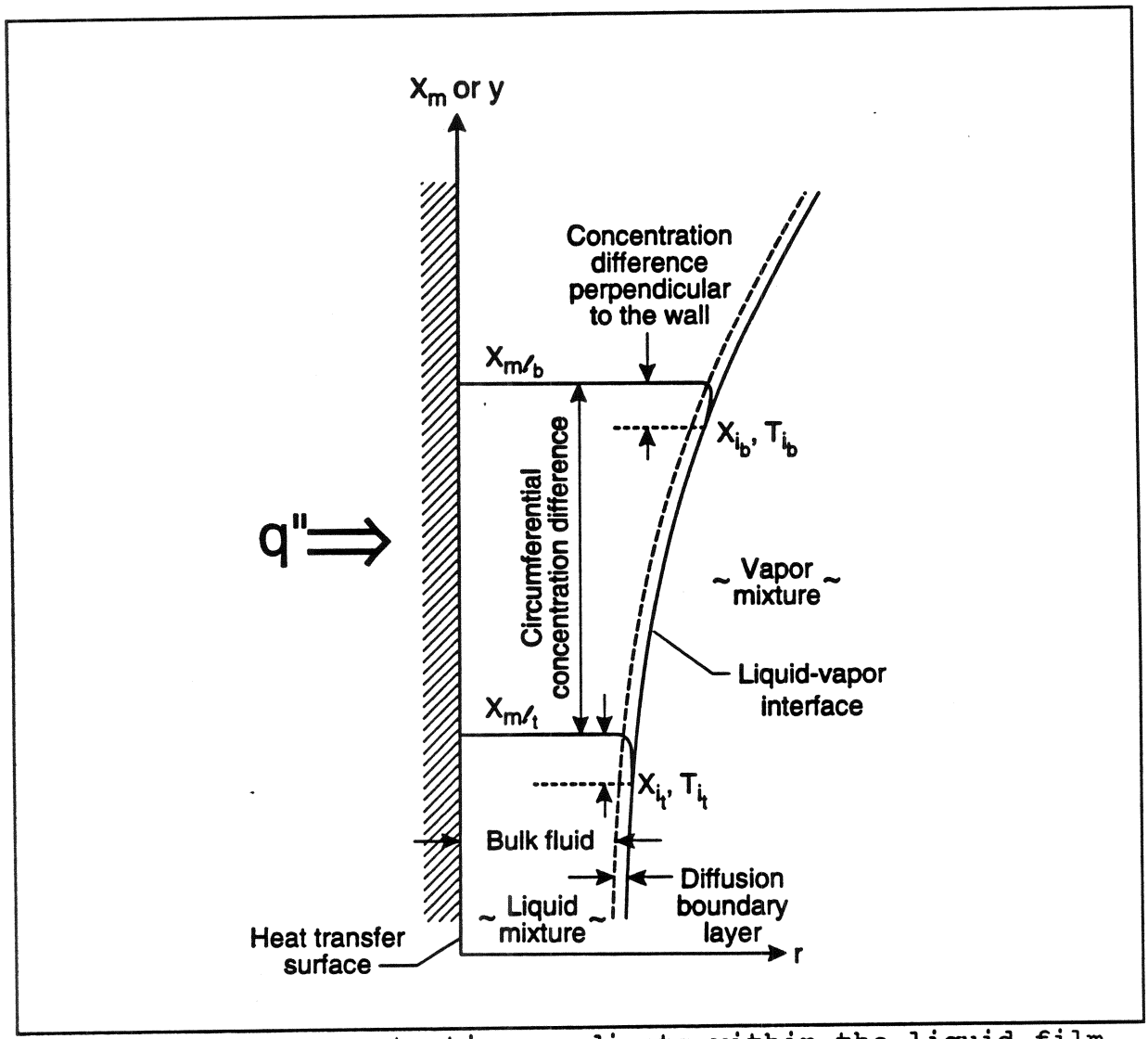

Figure 2-4 Concentration gradients within the liquid film

preferential evaporation of the more volatile component. Notice that there are concentration gradients in two directions: (1) parallel to the uniformly heated surface (dx_{ml}/dy), and (2) perpendicular to (or radially from) the uniformly heated surface (dx_{ml}/dr).

The concentration gradient parallel to the heated surface shown in Fig. 2-4 is induced by the constant heat flux boundary condition and the varying film thickness. As a mixture evaporates, the bulk

liquid is depleted of the more volatile component. In other words, an increase in the thermodynamic quality reduces the mass fraction of the more volatile component in the liquid mixture. The mass fraction coordinate is measured along the wall, increasing in the vertical y-direction. The mass fraction of the more volatile component in the thin-film (x_{mlt}) region is less than that of the thick-film (x_{mlb}) region. This is so because the thin-film region, having less mass but the same heat input, is at a higher effective, thermodynamic quality. Consequently, a film thickness gradient has induced a concentration gradient along the heated surface. Since gravity imposes a nonuniform circumferential film thickness distribution for horizontal annular flow, the above argument describes the mechanism of the circumferential concentration gradients for annular flow within a horizontal tube. The temperature of the liquid-vapor interface at the top of the tube (T_{it}) is greater than that at the bottom of the tube (T_{ib}). The magnitude of the liquid-vapor interface temperatures are determined by both the circumferential and the radial concentration gradients. The concentration gradient perpendicular to the heated surface exists primarily within the thickness of the diffusion boundary layer at the liquid-vapor interface, as shown in Fig. 2-4. Turbulent mixing prevents the formation of concentration gradients within the bulk liquid. In summary, evaporation depletes the diffusion boundary layer of the more volatile component, and the convection confines the concentration gradient to a narrow region within or close to the liquid-vapor interface. This describes the mechanism of the radial concentration gradients for annular flow within a horizontal tube.

Figure 2-5 demonstrates the variation of the two-phase heat transfer coefficient with respect to composition for an illustrative mixture. The dashed line represents experimental data. Notice that the heat transfer coefficient can be less than that for either pure component. The solid line, h_i, is a linear

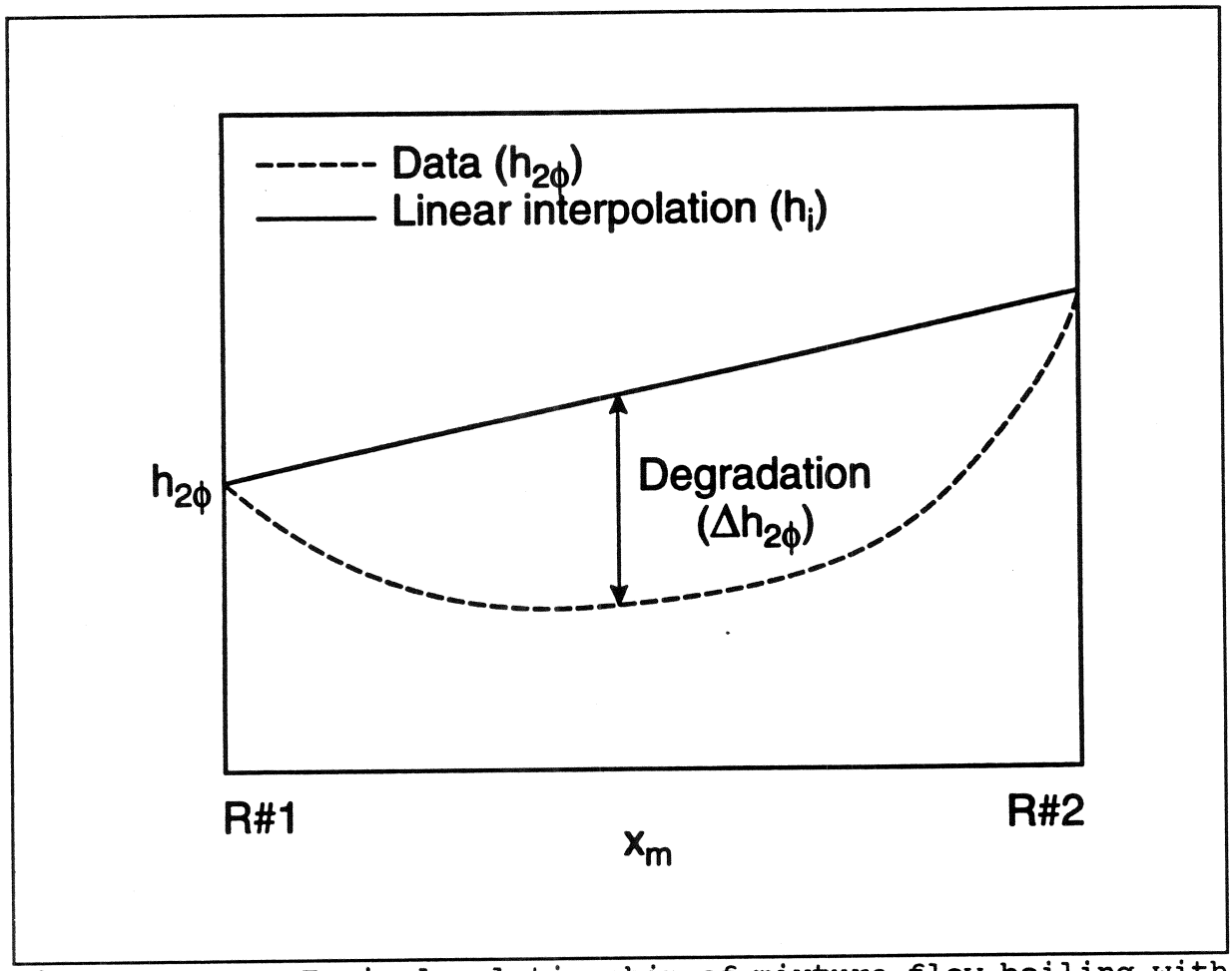

Figure 2-5 Typical relationship of mixture flow boiling with respect to composition

interpolation between the heat transfer coefficients of the pure components. The straight line has no physical meaning; however, it is used as a reference from which the degradation of the heat transfer coefficient of binary mixtures can be quantified. The heat transfer degradation ($\Delta h_{2\phi}$) is the difference between the interpolated heat transfer coefficient (h_i) and the measured heat transfer coefficient ($h_{2\phi}$) for a given composition.

Several explanations for the heat transfer degradation associated with mixtures have been postulated. Two popular reasons are the loss of available superheat and mass transfer resistance. Also,

Ross et al. [2], Jung and Didion [3] and Stephan and Preusser [4] attribute a portion of the degradation to the nonlinear variation of the thermodynamic and transport properties of mixtures with composition. The nonlinear variation of properties with respect to composition may contribute to a nonlinear degradation of the heat transfer coefficient. Stephan and Korner [5] suggest still another reason for the degradation: mixtures must do more work to form bubbles than an equivalent pure fluid.

Loss of available superheat, as described by Shock [6], is the loss of the heat transfer driving potential due to the increase of the fluid temperature upon evaporation. For a fixed tube-wall temperature, an increase in the fluid temperature results in a reduction or a loss of temperature difference between the wall and the fluid. The data examined here are for a constant, imposed heat flux boundary condition, not a constant wall temperature boundary condition. For the constant heat flux case, the heat transfer driving potential is the heat flux, which dictates the tube-wall temperature. A loss in driving potential cannot be imposed by an increase in fluid temperature upon evaporation since the wall temperature will rise, as the fluid temperature rises, to satisfy the imposed heat flux boundary condition. For the above reasons, the argument for the loss of available superheat does not strictly apply to the constant heat flux boundary condition and, consequently, cannot be investigated in this study.

Mass transfer, as defined in this paper, is the movement of a liquid component due solely to a concentration gradient. The motion of the liquid is induced by the tendency of the liquid to achieve a uniform equilibrium concentration. The magnitude of the mass flux due to mass transfer is insignificant compared to that due to evaporation by heat exchange. Therefore, mass transfer cannot significantly reduce the heat transfer by a movement of fluid which is opposed to the evaporation. However, mass transfer can indirectly affect the heat transfer by determining the

magnitude of the concentration gradients. In turn, the concentration gradients establish the temperature distributions which control the heat transfer. In summary, the mass transfer affects the heat transfer coefficient primarily by altering the temperature through concentration gradients and not by the movement of fluid.

Mass transfer resistance is defined in this paper as a resistance to the neutralization of concentration gradients. The mass transfer resistance indirectly causes a degradation in the heat transfer by raising the liquid temperatures. For clarity, concentration gradients rather than mass transfer resistance is used to discuss the heat transfer degradation.

The additional work of bubble formation cannot be studied in the convective region. All of the data which were examined are in the convective, evaporative flow region. Nucleate boiling is suppressed in the convective region [7]. Therefore, the additional resistance due to bubble formation in a mixture cannot be examined using the cited data.

For the above reasons, the focus of the investigation is on the effects of concentration gradients and nonlinear mixture properties on the heat transfer degradation. It cannot be known with any certainty that the above two effects are the only effects that contribute to the heat transfer degradation. However, it is assumed that the heat transfer degradation that is not due to the fluid property effect is due to concentration gradients.

For evaporative flow, it is speculated that most of the heat transfer degradation associated with concentration gradients results from the use of the saturated equilibrium temperature in the calculation of the heat transfer coefficient. If concentration gradients are present in the liquid, the actual liquid-vapor interface temperature (vapor temperature) will be greater than the

saturated equilibrium temperature which is obtained from an overall energy balance and the measured pressure. If the actual liquid-vapor interface temperature were used to calculate the measured heat transfer coefficient, the heat transfer coefficient would be greater than that calculated from the equilibrium temperature. Consequently, a large portion (possibly all) of the heat transfer degradation associated with concentration gradients can be attributed to the use of the equilibrium temperature in the calculation of the measured heat transfer coefficient.

Experimental Work Investigated

Only binary-mixture, horizontal-flow boiling with a constant tube wall heat flux is considered here [2,3,8,9]. The local two-phase heat transfer coefficient ($h_{2\phi}$) was calculated as:

$$h_{2\phi} = \frac{q''}{T_w - T_s} \tag{2-1}$$

where q" is the heat flux at the outside wall, T_w is the inside wall temperature, and T_s is the saturated fluid temperature evaluated at the measured pressure. Local wall temperature measurements were made along the tube length. The tube wall temperature was measured at four circumferential positions, 90 degrees apart, at each axial position along the tube. Four circumferential heat transfer coefficients (top, bottom, right, and left side) were calculated and averaged to obtain the value for the heat transfer coefficient at the given axial position.

Ross et al. [2] have measured the local flow boiling heat transfer coefficient for various compositions of the R13B1/R152a mixture. Figure 2-6 presents the measured two-phase heat transfer coefficient ($h_{2\phi}$) versus the mass fraction of the more volatile component, R13B1. The data of Fig. 2-6 were taken for a saturation temperature, at the exit of the test section, of 270 K, a mass flux of 460 kg/(m^2 s), a thermodynamic quality of 40%, and an incident heat flux of 30 kW/m^2. The solid line is a linear interpolation

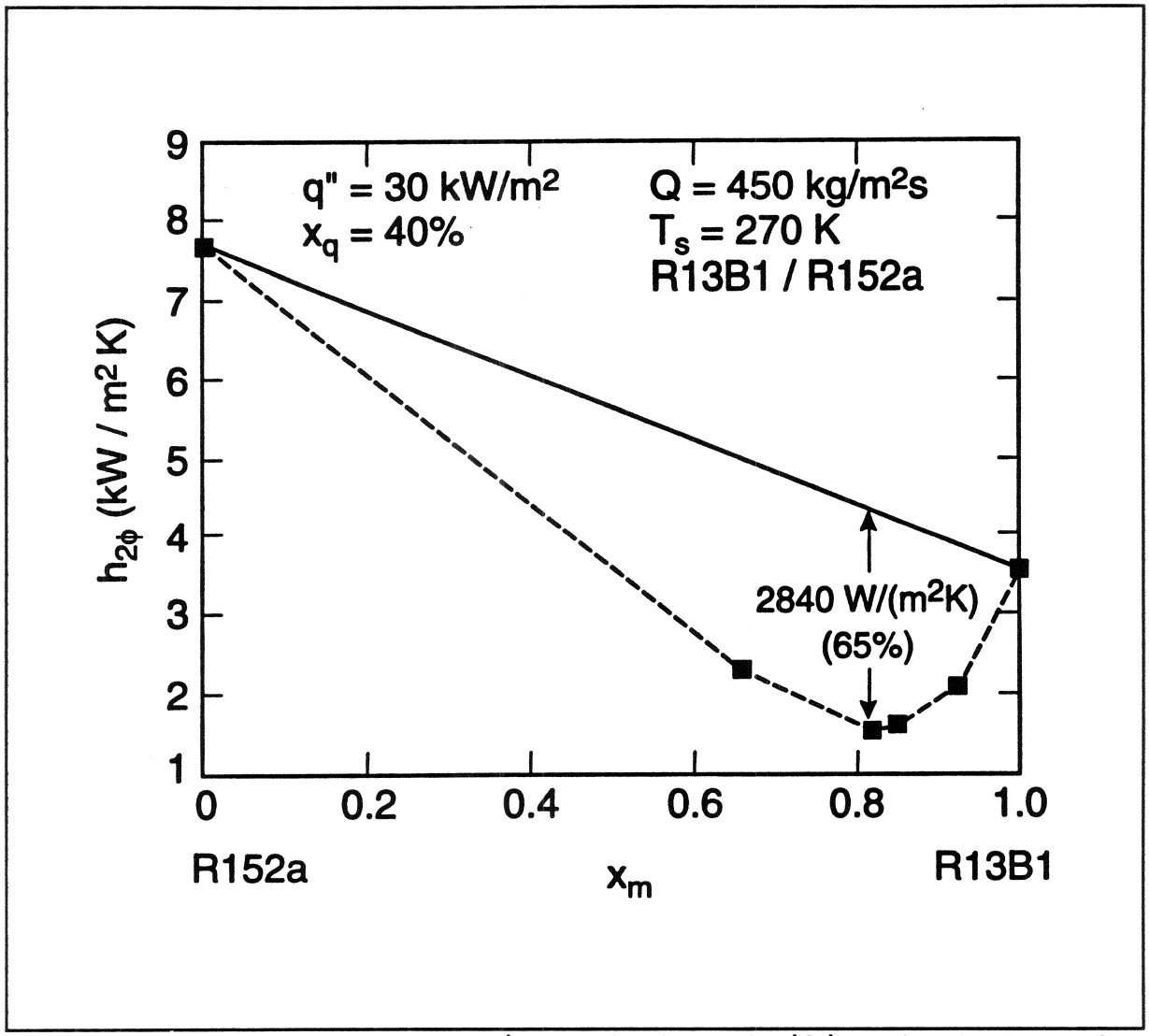

Figure 2-6 Measured horizontal flow boiling heat transfer coefficient for the R13B1/R152a mixture (Ross et al. (1987))

between the heat transfer coefficients for the single components. The degradation as compared to the single component reference line is greatest (65% of h_i) at x_m = 0.82.

Jung et al. [9] measured the local flow boiling heat transfer coefficient for various compositions of the R12/R152a mixture and the R22/R114 mixture. Their data for a reduced pressure (P_r) of 0.08 at the exit of the test section, a constant imposed heat flux

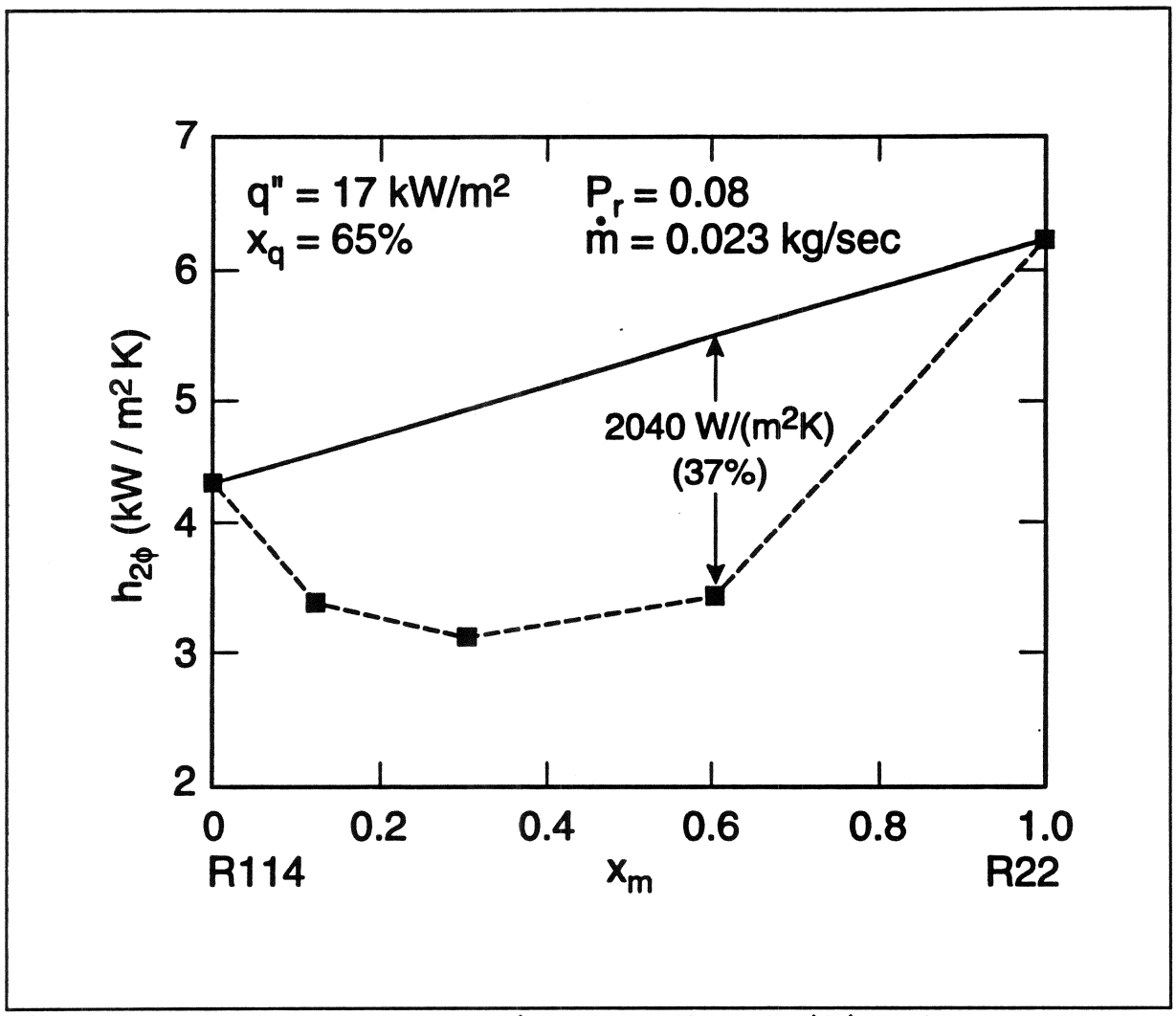

Figure 2-7 Measured horizontal flow boiling heat transfer coefficients for the R22/R114 mixture (Jung and Didion, 1989)

of 17 kW/m^2, a thermodynamic quality of 65%, and a mass flow rate ($\dot{m}$) of 0.023 kg/s are shown in Figs. 2-7 and 2-8. The maximum heat transfer degradation for the R22/R114 mixture is located at an overall mass composition of 0.61. Its magnitude is 2040 W/m^2-K or 37% lower than the linear interpolation between the $h_{2\phi}$ for the pure components.

The heat transfer degradation for the R22/R114 mixture is large,

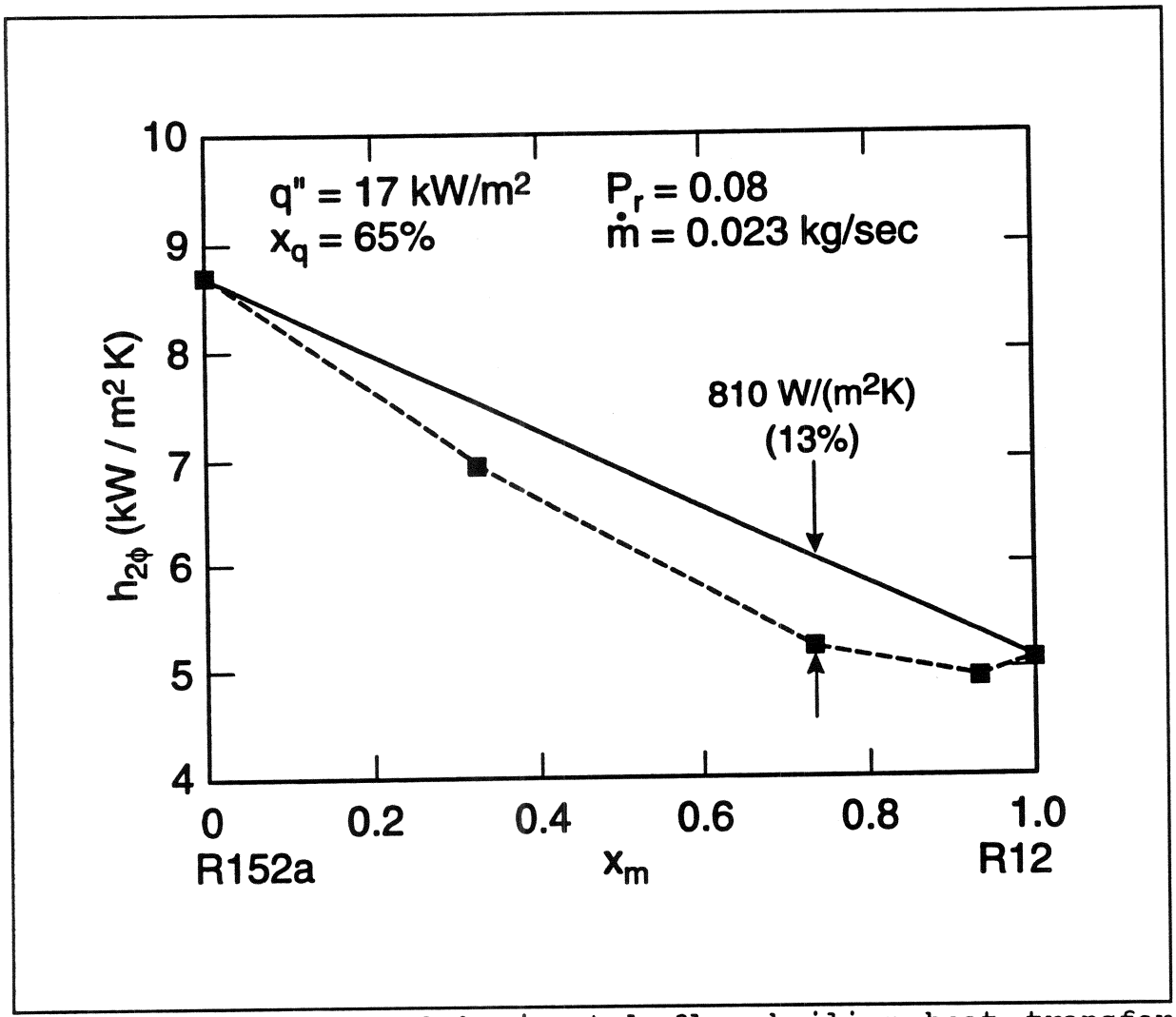

Figure 2-8 Measured horizontal flow boiling heat transfer coefficient for the R12/R152a mixture (Jung and Didion, 1989)

but not as large as that present for the R13B1/R152a mixture. It is intuitively reasonable to suggest that the large heat transfer degradation associated with the R13B1/R152a data is a result of the coupled effects of: (1) the large difference in mass concentration between the liquid and vapor phases ($x_{mv} - x_{ml} = 0.12$ at $x_m = 0.82$) and, (2) the relatively large molecular mass (149 g/mol) of the more volatile component (R13B1). The difference in concentration between the liquid and vapor phases represents the

potential for concentration gradients within the liquid. The difference between the vapor and liquid composition (x_{mv} - x_{ml}) for the R22/R114 mixture is approximately 0.02 mass fraction greater than that for the R13B1/R152a mixture from about 0.2 to 0.8 liquid mass fraction. Therefore, the potential for mass transfer resistance is slightly greater for the R22/R114 than it is for the R13B1/R152a mixture. However, the molecular mass of R22 is 86 g/mol, and that of R13B1 is 149 g/mol. In other words, the more volatile component of the R22/R114 mixture is lighter than that of the R13B1/R152a mixture. The speed at which molecules diffuse determines the magnitude of the concentration gradient [10]. For binary liquids, the rate of diffusion is primarily a function of: (1) the liquid viscosity, (2) the derivative of the log of the activity with respect to the log of the mole fraction of the more volatile component, and (3) the molecular mass of the components [11]. The viscosity and the activity-composition data for the two mixtures do not differ significantly. If an analogy with vapor diffusion is permitted, then it is reasonable to assume that heavy liquid molecules, like those of R13B1, would diffuse more slowly than the lighter R22 liquid molecules. Consequently, there would be larger concentration gradients present in the R13B1/R152a mixture than in the R22/R114 mixture. Therefore, it is hypothesized that the heat transfer degradation of the R13B1/R152a mixture is larger than that of the R22/R114 mixture because the molecular mass of the more volatile component of the R13B1/152a mixture is greater than that of the R22/R114 mixture.

The phase equilibrium diagram for the R12/R152a mixture, in Fig. 2-2, shows that the maximum difference between the liquid and vapor compositions for that mixture is approximately 0.1 mole fraction. The fact that the composition difference is small suggests that the potential for heat transfer degradation should be small. The measured two-phase heat transfer coefficient for the R12/R152a mixture, shown in Fig. 2-8, satisfies the speculation by exhibiting

only a 13% degradation in the heat transfer from the linear interpolation.

Effect of Fluid Properties on $h_{2\phi}$

Mixing Rules

The calculation of the heat transfer coefficient, as given by equation (1), requires relatively few fluid properties. However, its correlation and prediction rely heavily on the estimated or measured fluid properties. For this reason, it is essential that correlations are presented along with the fluid property mixing rules that were used to fit the data. The following analysis demonstrates the effect of the mixing rule on the determination of the two-phase heat transfer coefficient for mixtures in the convection-dominated regime.

The functional form of the Dittus-Boelter [12] equation[$(k_l^{0.6}(c_{pl}/\mu_l)^{0.4})\rho_l^{0.8}$] is frequently used to correlate the convection-dominated region of two-phase flow within a tube. The k_l is the thermal conductivity of the liquid; c_{pl} is the specific heat of the liquid; μ_l is the viscosity of the liquid; and, ρ_l is the density of the liquid. These are the primary fluid properties which are necessary for the correlation and prediction of heat transfer coefficients for two-phase flow boiling.

An estimate of the fluid properties of a mixture can be obtained from the fluid properties of the pure components using mixing rules. Three typical mixing rules are: (1) linear, (2) ideal, and (3) non-ideal. The simplicity of the linear mixing or mass fraction averaging rules is attractive:

$$k_{l_m} = x_{m_1} k_{l_1} + (1 - x_{m_1}) k_{l_2} \qquad (2\text{-}2)$$

$$c_{p_{l_m}} = x_{m_1} c_{p_{l_1}} + (1 - x_{m_1}) c_{p_{l_2}} \qquad (2\text{-}3)$$

$$\mu_{l_m} = x_{m_1}\mu_{l_1} + (1 - x_{m_1})\mu_{l_2} \tag{2-4}$$

Linear mass fraction weighing mixing rules are seldom used to approximate the liquid thermal conductivity and the liquid viscosity. However, the linear mixing rule can be used to closely approximate the specific heat of a mixture.

The ideal mixing rules are slightly more complex than the linear mixing rules, but closely approximate the properties of a mixture where the pure components have similar vapor pressures and come from similar chemical families. The ideal mixing rules assume that there are no mixing effects that enhance or reduce the value of the property due to mixing [13].

$$k_{l_m} = \exp[x_{m_1}\ln(k_{l_1}) + (1 - x_{m_1})\ln(k_{l_2})] \tag{2-5}$$

$$\mu_{l_m} = \exp[x_{m_1}\ln(\mu_{l_1}) + (1 - x_{m_1})\ln(\mu_{l_2})] \tag{2-6}$$

The non-ideal mixing rules chosen for this study have an additional term to account for the effects of mixing:

$$k_{l_m} = x_{m_1}k_{l_1} + (1 - x_{m_1})k_{l_2} - 0.72x_{m_1}(1 - x_{m_1})\,|k_{l_1} - k_{l_2}| \tag{2-7}$$

$$\begin{aligned}\mu_{l_m} = {} & \exp[x\ln(\mu_{l_1}) + (1 - x)\ln(\mu_{l_2})] \\ & + 0.85[\rho_{l_{exp}}(\frac{x}{\rho_{l_1}} + \frac{(1-x)}{\rho_{l_2}}) - 1] - 0.085\end{aligned} \tag{2-8}$$

Equation (2-7) was obtained from Reid et al. [13], and equation (2-8) was obtained from Jung and Didion [14].

Figure 2-9 is used to examine the impact of the mixing rule on the prediction of the heat transfer coefficient for mixtures. The figure consists of four graphs of the predicted $h_{2\phi}$ versus the mass fraction (x_m) for the R22/R114 mixture. The uppermost line is the

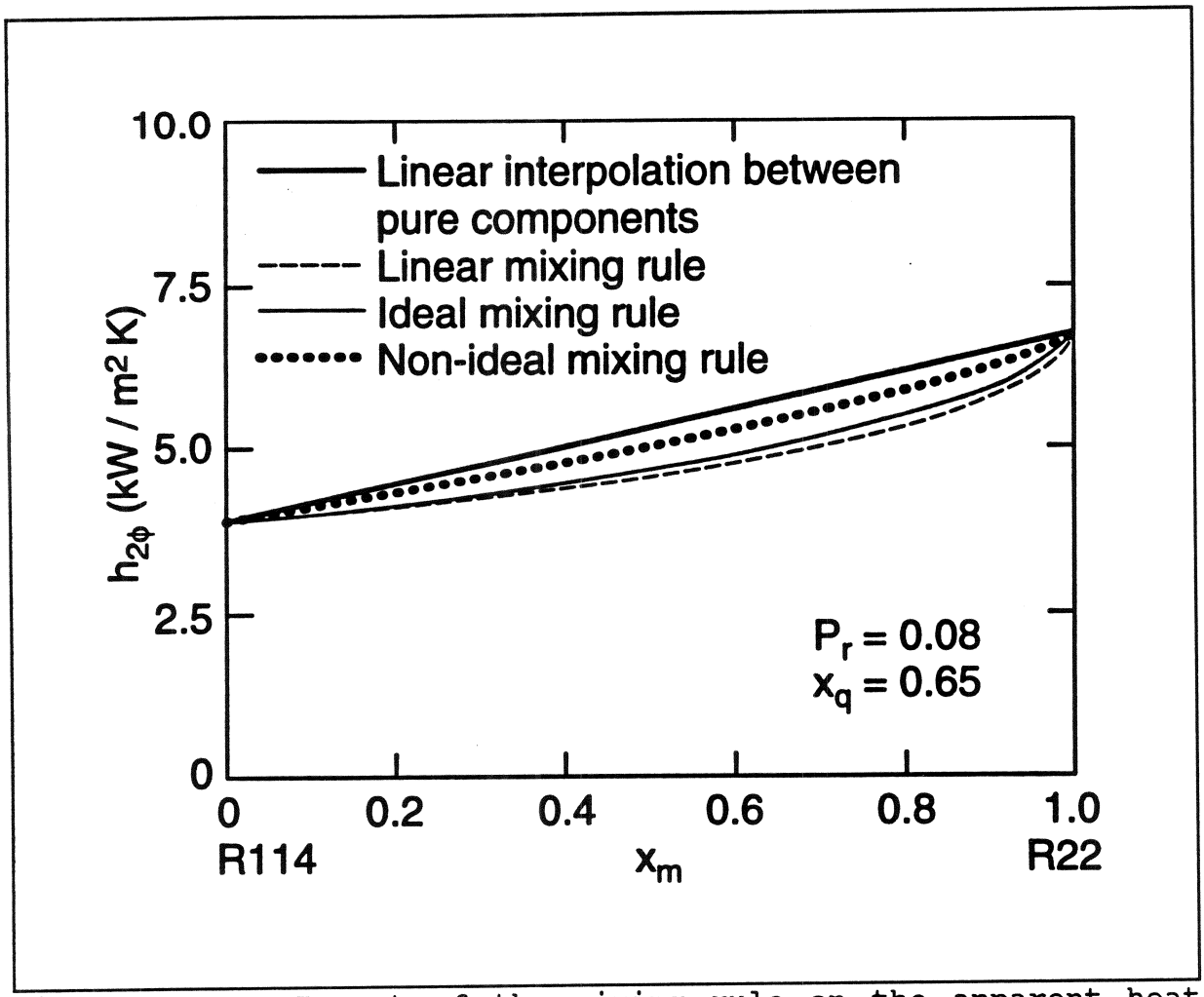

Figure 2-9 Impact of the mixing rule on the apparent heat transfer degradation of the R22/R114 mixture

linear interpolation between the heat transfer coefficients of the single components, R22 and R114. The remaining three graphs are of the predicted flow boiling heat transfer coefficient (h_p). Three different mixing rules are used to estimate the fluid properties in the correlation. Jung's [3] flow boiling correlation for single component fluids was used so that only the effect of the mixing rule on the heat transfer coefficient was examined. The predictions can be viewed as a heat transfer coefficient for the mixture if there were no concentration gradients present within the liquid.

Three general characteristics of Fig. 2-9 are evident. First, note that the predicted heat transfer coefficient is nonlinear with respect to the composition for all of the mixing rules. Second, the apparent heat transfer degradation is the greatest at a mass fraction of 70%, which is different from the mass fraction for the greatest value of $x_{mv} - x_{ml}$. This indicates that the nonlinear property effects are acting to degrade the heat transfer by a mechanism which is different from that of the concentration gradient effects. The consequence of the property effects interacting with the concentration gradient effects is to minimize the heat transfer at a composition which is a compromise between the two effects. Third, the apparent maximum heat transfer degradation becomes less as the mixing rule for the fluid property estimations progress from the linear to the ideal and finally, to the non-ideal. In summary, the maximum deviation from the linear interpolation is 18% for the linear mixing rule, 14% for the ideal mixing rule, and 6% for the non-ideal mixing rule. Figure 2-9 demonstrates the importance of consistency in the use of mixing rules for estimating the fluid properties to be used in the heat transfer coefficient correlations.

The Less Volatile Components

The removal of heat from the wall by convection for two-phase flow within a tube is governed by both the molecular conduction of heat through the liquid film and the transport of the liquid along the tube wall. Hence, the local properties of the liquid film determine the local rate of heat transfer. Figure 2-3 illustrates that the composition of the liquid increases in the less volatile component as the fluid evaporates. For this reason, care should be taken to evaluate the liquid properties at the liquid composition (x_{ml}) (not the overall composition (x_m)) in both the correlation and prediction of the flow boiling heat transfer coefficient with respect to flow quality (x_q).

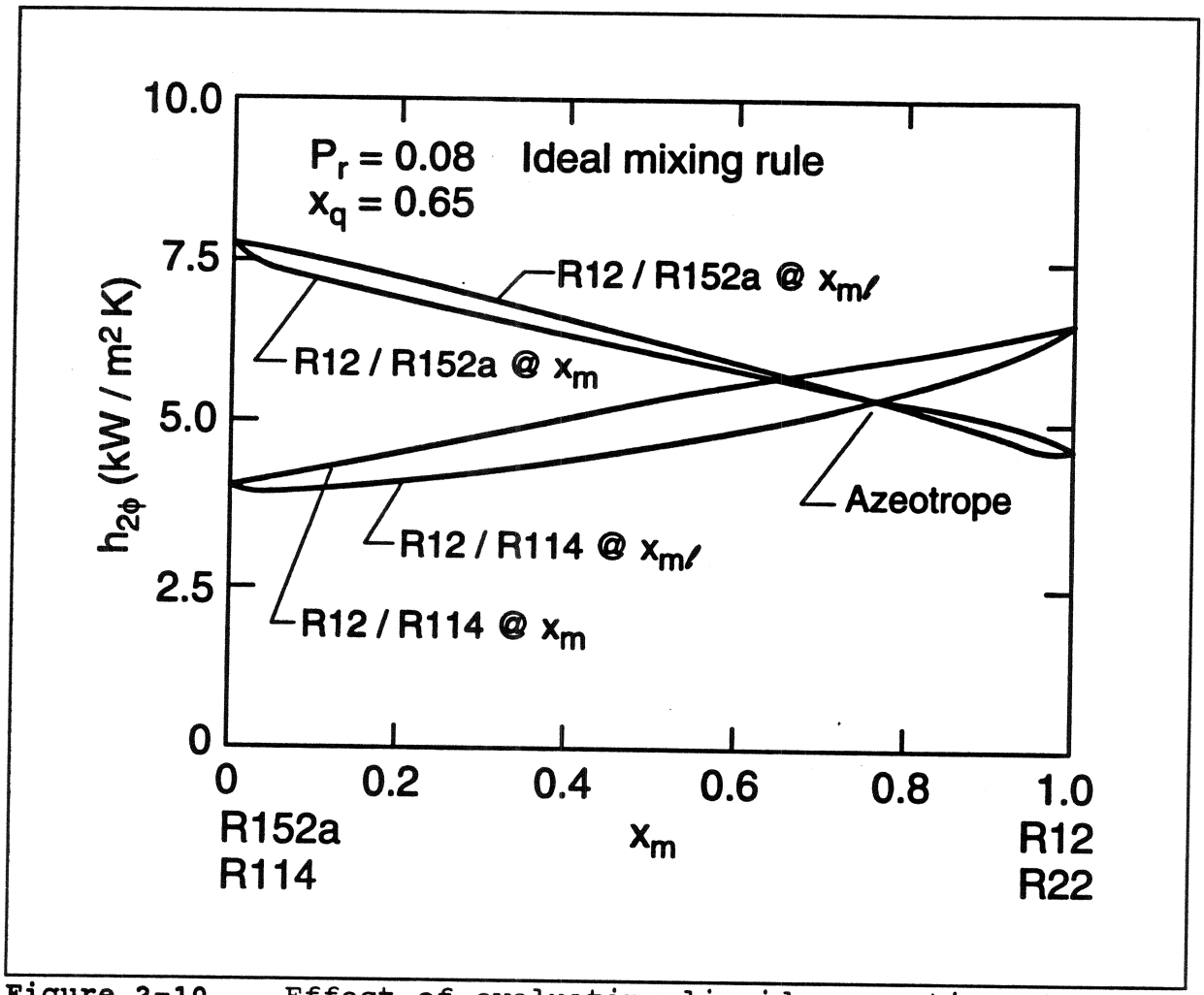

Figure 2-10 Effect of evaluating liquid properties at x_m and x_{ml} on $h_{2\phi}$

Figure 2-10 is a plot of the predicted heat transfer coefficient, using Jung's [3] single component model, versus the overall composition. The figure shows that as large as a 15% error in the prediction of the heat transfer coefficient can occur if the fluid properties are evaluated at the overall composition rather than the liquid composition. The heat transfer coefficient for the R12/R152a mixture will be underestimated by using the overall composition to evaluate the liquid properties. Contrary to this, the heat transfer coefficient for the R22/R114 mixture will be overestimated by using the overall composition to evaluate the liquid properties.

In general, the liquid properties of a two-phase mixture more closely resemble those of the less volatile component than that which would be anticipated considering the overall composition. For a R22/R114 mixture, this results in heat transfer coefficients which are always below the linear interpolation of the heat transfer coefficients of the single components. However, the predicted heat transfer coefficients evaluated at x_{ml} for the R12/152a mixture are slightly above the h_i values. The liquid properties of R152a are more beneficial for convection than the liquid properties of R12, resulting in an enhancement with respect to the overall composition. The opposite is true for the R22/R114 mixture where the liquid properties of the less volatile component do not promote the convection as well as the more volatile component. It may be possible to tailor a mixture which has heat transfer coefficients above the linearly interpolated values by selecting the less volatile component to have the best convective characteristics of all the components.

Components of Degradation

Following is an attempt to isolate and quantify the individual components of the total heat transfer degradation depicted in Fig. 2-5. The first section concentrates on determining the influences of fluid properties and liquid concentration gradients on the heat transfer coefficient. The last section attempts to isolate the proportions of the $\Delta h_{2\phi}$ that are due to the circumferential and radial concentration gradients.

In order to analyze the influence of fluid properties on the heat transfer coefficient in the absence of concentration gradients, the correlation for two-phase single component horizontal flow boiling by Jung and Didion [3] was utilized. Figure 2-11 shows the two-phase heat transfer coefficient for the R12/R152a mixture, as predicted using the Jung and Didion [3] correlation, versus the mass fraction of the more volatile component. The predicted values

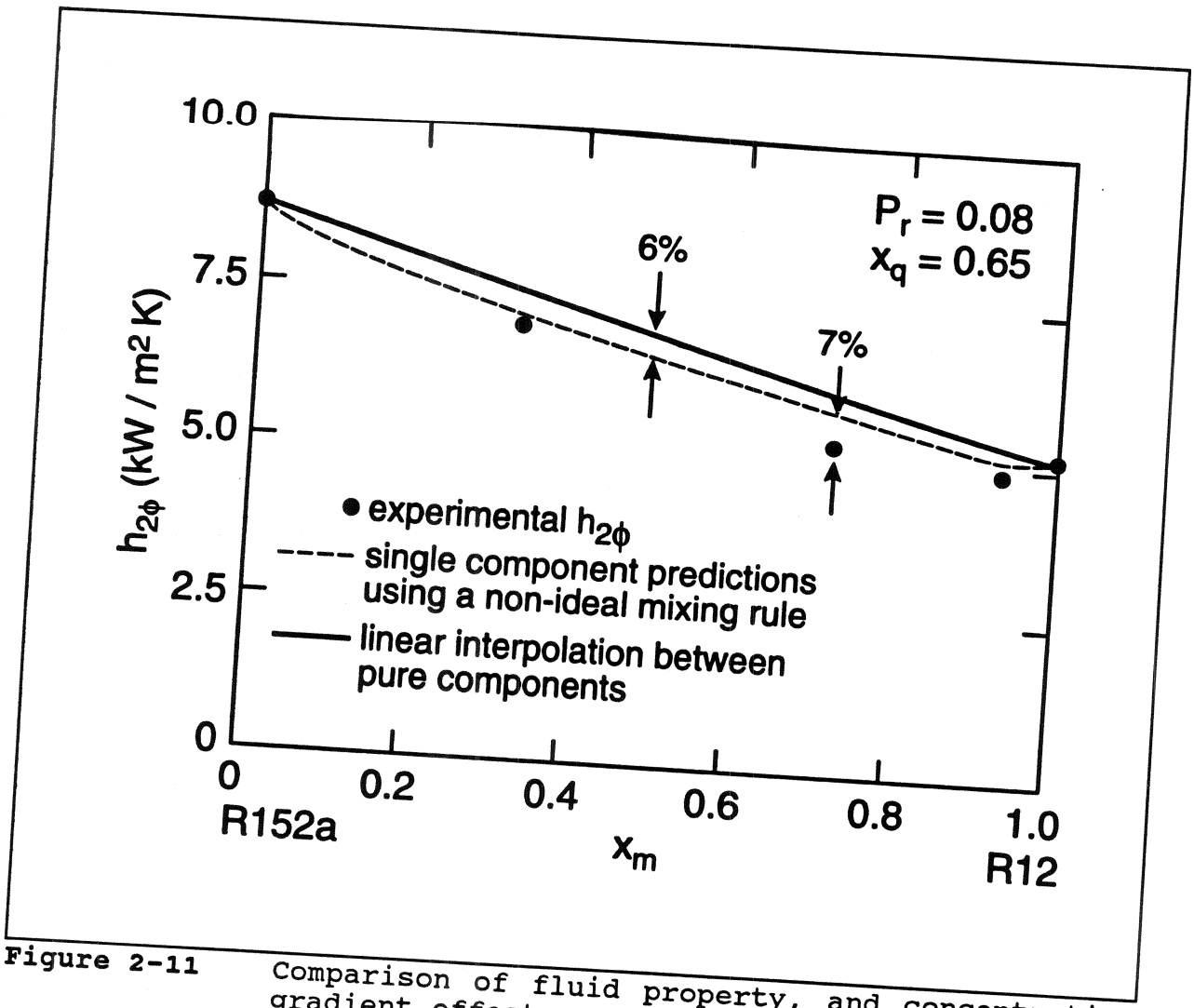

Figure 2-11 Comparison of fluid property, and concentration gradient effects on the degradation of R12/R152a heat transfer

mass fraction of the more volatile component. The predicted values were adjusted to facilitate a fair analysis of the nonlinear property effects on the heat transfer. The difference between the prediction and the linear interpolation between the predicted single component heat transfer coefficients was transferred to Fig. 2-11 as a heat transfer degradation for the measured heat transfer coefficients due to nonlinear property effects. Figure 2-11 compares the experimental data to the adjusted predicted values for the R12/R152a mixture. The fluid properties degrade the heat transfer coefficient by 6% at x_m = 0.5. Concentration gradients